Metabolic homeostasis controls the diversity of cooperative swarming in pathogenic bacteria

Guillem Santamaria[1,3+], Chen Liao[1+], Zhe Wang[2], Kyu Rhee[2], Francisco Pinto[3], Jinyuan Yan[1]*, Joao B. Xavier[1]*

[1]Program for Computational and Systems Biology, Memorial Sloan-Kettering Cancer Center, New York, NY, USA

[2]Department of Medicine, Weill Cornell Medical College, New York, NY

[3]BioISI – Biosystems & Integrative Sciences Institute, Faculty of Sciences, University of Lisboa, Lisboa, Portugal

[+]these authors contributed equally

[*]Correspondence: yanj2@mskcc.org and xavierj@mskcc.org

Abstract

Many bacteria have an incredible ability to swarm cooperatively over surfaces. But swarming phenotypes can be quite different even between strains of the same species. What drives this diversity? We compared the metabolomes of 29 clinical *Pseudomonas aeruginosa* isolates with a range of swarming phenotypes. We identified that isolates incapable of secreting rhamnolipids—a surfactant needed for swarming—had perturbed tricarboxylic acid (TCA) cycle and amino acid pathways and grew exponentially slower in glycerol minimal medium. Analysis of the metabolome signatures and simulations using a genome-scale model led to a mechanism which joins these observations: Strains subject to higher oxidative stress levels grow slower and shut down rhamnolipids secretion, a carbon overflow mechanism possibly to direct carbon resources towards costly stress response pathways to maintain cell viability. *In vitro* experiments confirmed that rhamnolipid non-producers deal worse with oxidative stress, linking intracellular redox homeostasis—a individual-level trait—to swarming—a population-level behavior. This mechanism helps explain the metabolic constraints on bacteria when secreting byproducts to interact with others—competitively and cooperatively—in microbial communities.

Significance

Swarming motility has been associated with virulence of many human bacterial pathogens. The pathogen *Pseudomonas aeruginosa* swarms by cooperatively secreting surfactants called rhamnolipids to lubricate surfaces. To understand why some *P. aeruginosa* strains swarm and others do not, we combined metabolomics, computational modeling and *in vitro* experiments to study the different swarming behaviors of 29 isolates of *Pseudomonas aeruginosa* obtained from infected patients. We found that strains can only produce rhamnolipids if they can maintain redox homeostasis. We propose that single cells must have low internal redox stress

levels before they can produce rhamnolipids, which work as an overflow of carbon metabolism into a cooperative secretion that brings a fitness benefit to the entire swarming population. This mechanism links single-cell physiology and a population-level cooperative behavior key to the fitness and virulence of *P. aeruginosa*, a major source of hospital acquired infections.

Synopsis

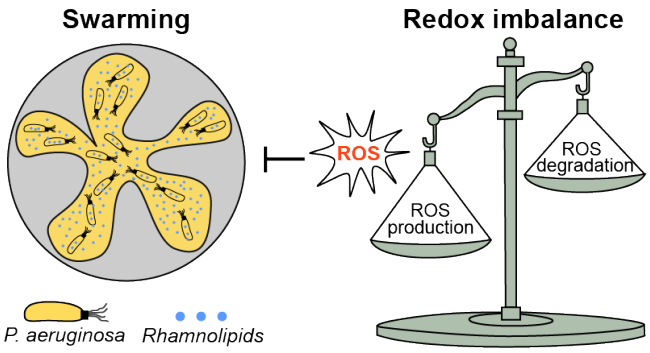

This study combined metabolomics, computational modeling and experiments to explain the swarming diversity in *Pseudomonas aeruginosa*, yielding new insights on the genetic and metabolic controls of bacterial swarming behavior

- Rhamnolipid secretion is necessary, but insufficient, for swarming
- *P. aeruginosa* strains unable to produce rhamnolipids in the glycerol minimal medium have perturbed metabolism, slow growth and elevated oxidative stress
- Rhamnolipid producers cannot produce rhamnolipids in succinate as the sole carbon source which causes greater ROS (reactive oxygen species) production
- The requirement of redox homeostasis for rhamnolipid production ensures that the overflow of precious carbon for population-level benefit is prudently controlled
- This study helps linking single cell physiology with collective behavior key to the fitness and virulence of a pathogenic bacterium.

57 **Introduction**

58 Swarming enables millions of bacteria to travel together across centimeter-long distances in a
59 few hours (Deforet *et al*, 2014). This cooperative trait found typically in the phyla Alpha-
60 proteobacteria and Gamma-proteobacteria is a complex phenotype that requires the
61 coordinated expression of many genes: Swarming requires flagella or pili to propel the cells,
62 cell-cell interactions to maintain population integrity during migration, and the collective
63 secretion of biosurfactants to lubricate the surface (Kearns, 2010). Studies over the past two
64 decades revealed many molecular details of swarming motility through genetic (e.g.,
65 knockouts, transgenesis) and environmental (e.g., nutrient composition and viscosity of
66 culture medium) perturbations (Köhler *et al*, 2000; Mattingly *et al*, 2018) as well as through
67 experimental evolution (van Ditmarsch *et al*, 2013). Some genes that modulate swarming
68 impact key cellular activities including tricarboxylic acid (TCA) cycle and stress response
69 (Inoue *et al*, 2007; Tremblay & Déziel, 2010) and therefore have pleiotropic effects. Despite
70 these insights, we lack a systems-level understanding of this cooperative bacterial behavior
71 (Kim & Surette, 2004; Inoue *et al*, 2007).

72 *Pseudomonas aeruginosa*—an opportunistic human pathogen and a major cause of hospital-
73 acquired infections (Klevens *et al*, 2007)—has a remarkable swarming ability that produces
74 long straight segments (tendrils) in its fractal-like swarming pattern. Similar to other
75 swarming species, *P. aeruginosa* requires both flagella and pili to move, the LasR-LasI and
76 RhlR-RhlI quorum sensing systems to communicate within population, and the ability to
77 produce rhamnolipids to lubricate the surface (Köhler *et al*, 2000). Rhamnolipids are a
78 mixture of biosurfactants that consist of 3-(3-hydroxyalkanoyloxy) alkanoic acids (HAAs),
79 mono-rhamnolipids and di-rhamnolipids (Abdel-Mawgoud *et al*, 2010). RhlA is the only
80 enzyme required to drive the conversion of fatty acid biosynthesis intermediates (β-

81 hydroxyacyl-ACP) to HAAs (Zhu & Rock, 2008), whereas RhlB and RhlC each add one
82 molecule of rhamnose to the HAAs to produce mono-rhamnolipids and di-rhamnolipids in
83 sequential steps (Chong & Li, 2017). The genes encoding RhlA and RhlB are located in the
84 same operon *rhlAB*, which is regulated by the quorum-sensing cascade headed by LasR-LasI
85 and followed by RhlR-RhlI (Medina *et al*, 2003). Other than quorum-sensing signals, *rhlAB*
86 expression is also controlled by nutrient cues such as an excess of carbon source (Xavier *et*
87 *al*, 2011; Boyle *et al*, 2015; Mellbye & Schuster, 2014). The combination of quorum-sensing
88 and metabolic signals is called metabolic prudence; it prevents cheating by rhamnolipid non-
89 producers such as the Δ*rhlA* mutant because it prudently ensures that rhamnolipids are only
90 produced at the right time when the production benefits outweigh its costs. Strains that
91 produce rhamnolipids too soon or overproduce rhamnolipids, such as a strain engineered with
92 the inducible P_{BAD}-*rhlA* construct, have less carbon available for growth and are susceptible
93 to cheating by non-producers (Xavier *et al*, 2011; de Vargas Roditi *et al*, 2013).

94 Besides the role of metabolic prudence, which regulates rhamnolipid production and makes
95 swarming robust to cheating, other aspects of metabolism might have influenced the
96 evolution of swarming across the *P. aeruginosa* phylogenetic tree. Metabolism is the
97 currency of all physiological processes that support life (Smith & Morowitz, 2004) and a
98 major determinant of social behavior (Biro & Stamps, 2010). A previous study (Boyle *et al*,
99 2017) compared the intracellular metabolites of the laboratory strain PA14 and several
100 mutants of that strain with different swarming phenotypes. The Δ*rhlA* mutant can neither
101 swarm nor produce rhamnolipids, but it had less than 10 metabolites perturbed compared to
102 the wild-type. The Δ*cbrA* mutant, which lacks a global regulator of carbon-nitrogen balance,
103 had impaired swarming and lower growth rate with dozens of perturbed metabolites. Notably,
104 the Δ*cbrA* mutant still had the flagella needed to move and secreted even more rhamnolipids
105 than the wild-type. More interestingly, its swarming phenotype could be rescued by

106 compensatory point mutations in the RNA chaperone *hfq* through rewiring of metabolic
107 network to reconstruct a unique metabolome which was distinct from both the Δ*cbrA* and the
108 wild-type (Boyle *et al*, 2017).

109 Here we leveraged a collection of 29 clinical isolates of *P. aeruginosa* that we previously
110 isolated from hospitalized cancer patients in Memorial Sloan-Kettering Cancer Center
111 (MSKCC) (Yan *et al*, 2017). These strains span a wide range of swarming phenotypes;
112 however, they evolved independently in environments that are largely unknown to us and
113 exhibit great genetic diversity, which makes it hard to pin down the exact genes responsible
114 for their different swarming behaviors. Since the differences cannot be solely explained by
115 genetics, here, in this study, we combined genomics with metabolomics, growth curve
116 analysis and computational models to study the metabolic differences underlying the
117 observed swarming diversity. Swarming requires rhamnolipid production; here we found that
118 rhamnolipid-producing strains have reduced TCA cycle activity, increased levels of amino
119 acids, and slower exponential-phase growth rate compared to the non-producing strains. We
120 further provided both computational and experimental evidences showing that these
121 metabolic changes are likely caused by a higher oxidative stress. This finding suggests that
122 rhamnolipid production is a form of overflow metabolism that is only activated in strains with
123 sufficient capability to detoxify reactive oxygen species (ROS) produced by energy
124 metabolism and maintain redox balance. This mechanism links redox homeostasis with
125 swarming cooperation, highlighting the importance of metabolism in the evolution of a social
126 behavior.

127 ## Results

128 **Phylogenetic analysis suggests loss of rhamnolipid production drove loss of swarming in**
129 **some isolates.** We started by analyzing the shapes of swarming colonies of clinical isolates

130 and three common reference strains whose genomes vary widely (Fig. 1). We used image
131 analysis to measure six morphological features of the colonies, including perimeter,
132 maximum length, area, circularity, skeleton longitude and eccentricity (see **Materials and**
133 **methods** for their definitions). A principal component analysis of these morphological
134 features revealed that the maximum length and circularity captured the most variability of the
135 shape diversity in our tested strains (Supplementary Fig. 1). We quantified the swarming
136 ability of all strains using a linear combination of the two features but found no significant
137 correlation of the swarming scores with the phylogeny inferred from their core genomes
138 (Moran's I test, p-value=0.93). Since production of rhamnolipids is required for swarming
139 motility, we measured the ability of strains to produce rhamnolipids in a synthetic media with
140 glycerol as the sole carbon source (Boyle *et al*, 2015). As expected, all strains able to swarm
141 produced rhamnolipids. Not all rhamnolipid producers swarmed, though, which confirms that
142 rhamnolipids are necessary but not sufficient for swarming (Caiazza *et al*, 2005; Déziel *et al*,
143 2003). Similar to swarming phenotype, the ability to produce rhamnolipids, semi-
144 quantitatively classified as non-, mild- and strong-producers (**Materials and Methods**), was
145 also uncorrelated with the phylogeny (Fig. 1B**,** Moran's I test, p-value=0.14). To better assess
146 the link between swarming and rhamnolipid production, we built an evolutionary model to
147 reconstruct their ancestral states along the phylogenetic tree. The model predicted that the
148 common ancestor of all the strains can both swarm and produce rhamnolipids. This prediction
149 suggests that the diversity of swarming found across the isolates was caused by some strains
150 losing their ability to swarm or produce rhamnolipids, not by concurrent lineages evolving
151 those functions independently. The model also suggests that rhamnolipid production is more
152 conserved than swarming: the immediate ancestors of all non-producers are inferred to be
153 rhamnolipid producers (Supplementary Figure 2A). By contrast, the loss of swarming
154 occurred earlier than that of rhamnolipid production in several lineages (Supplementary

155 Figure 2B), a result which is also expected because swarming depends on other factors
156 besides rhamnolipid production (Kearns, 2010).

157 **The loss of rhamnolipid production is partially explained by the absence of genes.** Since
158 the phylogeny inferred from core genes was unable to explain the observed diversity of
159 rhamnolipid production, we asked whether accessory genes, particularly those only missing
160 in rhamnolipid non-producers, could explain the diversity. Here we focused on the
161 comparison between rhamnolipid producers (both mild and strong rhamnolipid-producing
162 strains; the same below) and non-producers, rather than between swarmers and non-
163 swarmers, because (1) the latter phenotype is harder to determine non-arbitrarily and (2)
164 rhamnolipid production is itself a predictor of swarming (all rhamnolipid non-producers lose
165 swarming). We then compared the genomic sequences between the 8 rhamnolipid non-
166 producers and the remaining producers using reciprocal blast to explore the genetic features
167 that may be associated with rhamnolipid production. We identified 304 genes
168 (Supplementary File 1) only absent in those non-producers that may directly contribute to the
169 loss of rhamnolipid production (89 well annotated genes are listed in Table 1): F5677 lacks
170 the flagella motor switch protein *fliM*, and *qscR*—a quorum-sensing control repressor;
171 W36662 lacks the type IV pili assembly protein *pilC* and its sensor kinase *pilS*; and F63912,
172 W36662, W60856 lack three quorum-sensing genes *lasR*, *rhlR*, and *rhlI*. It was previously
173 shown that the single-gene knockout mutants Δ*fliM*, Δ*pilS*, Δ*rhlR* and Δ*rhlI* (Köhler *et al*,
174 2000; Overhage *et al*, 2007; Kamatkar & Shrout, 2011), but not Δ*pilC* (Luo *et al*, 2015),
175 displayed strong swarming-deficient phenotypes. The mutant of a two-component response
176 regulator gene *pirR* that is missing in H27930 was found to repress swarming in multiple
177 culture media (Kollaran *et al*, 2019). S86968 lacks *nfxB*, whose mutation caused global
178 dysregulation of physiology and metabolism in *P. aeruginosa* including impaired swarming
179 (Stickland *et al*, 2010). Notably, genes encoding rhamnolipid biosynthsis (*rhlA*, *rhlB*, *rhlC*)

180 are intact and contain no mutation in all non-producers, indicating that the mutations that lead
181 to the loss of rhamnolipid production are linked to the regulation of the pathway, either in
182 other regulatory genes (in coding or non coding regions) or in non-coding regions of the
183 biosynthetic genes.

184 Besides these functions that are directly linked to rhamnolipid production and swarming,
185 genes involved in carbon catabolism, biofilm, chemotaxis, antibiotic resistance, virulence and
186 redox regulation were also found missing in rhamnolipid non-producers. M55212 misses the
187 catabolite repression control gene *crc*, although a *crc* transposon mutant is able to swarm as
188 well as the wild-type (Yeung *et al*, 2011). H27930 lacks the methyl-accepting chemotaxis
189 genes *pctA* and *pctB* and the biofilm biosynthesis gene *pelA*. Both M1608 and S86968 lack
190 the pyridoxal phosphate (vitamin B_6) biosynthetic gene *pdxA* and the *hcnABC* genes coding
191 for the virulence factors hydrogen cyanide (Pessi & Haas, 2000). F5677 cannot express
192 PhzA2 for biosynthesis of phenazine—a well-known virulence factor. The absence of *amrB*
193 that encodes a membrane protein of the AmrAB-mediated efflux system in M1608 suggests
194 that the strain may be sensitive to the aminoglycoside antibiotic (Westbrock-Wadman *et al*,
195 1999). The missing genes for redox regulation include *soxR* (absent in F5677)—a redox
196 sensitive transcriptional regulator, *katE* (absent in M1608)—a catalase that degrades H_2O_2
197 (Mulvey *et al*, 1988), and *gor* (absent in M1608)—a flavoprotein that oxidizes glutathione,
198 which plays an important role in protection against H_2O_2 damage (Perry *et al*, 1991).

199 **Rhamnolipid producers grow faster in glycerol.** The missing genes in the 8 non-
200 rhamnolipid-producers (Table 1) include several global transcriptional regulators (e.g., *rhlR*,
201 *lasR*, *crc*, *nfxB*, *soxR*) that are broadly important for cell metabolism and growth. Their
202 absence may cause growth-independent or -dependent metabolic effects on rhamnolipid
203 production and swarming. We first tested whether growth is a predictor for the observed

204 diversity. We monitored growth curves of all our strains over 48h in the same glycerol media
205 that we had used to measure rhamnolipid production. These growth curves exhibited
206 markedly different lag times and exponential growth-rates (Fig. 1C), but a high similarity was
207 observed among 6 out of 9 swarming strains (Supplementary Fig. 3). However, some
208 rhamnolipid producers clustered with non-producers, suggesting that rhamnolipid production
209 cannot be classified by the entire growth curves and more sophisticated methods to extract
210 local growth curve features were needed.

211 We then used both unsupervised and supervised learning approaches to identify features in
212 the growth curves associated with rhamnolipid production. For the unsupervised approach,
213 we used non-negative matrix factorization (Lee & Seung, 1999) which decomposed each
214 growth curve as a weighted sum of three basis functions (i.e., features). Although the growth
215 curves of the rhamnolipid producers (orange lines) and non-producers (blue lines) largely
216 overlapped (Fig. 2A), there was a significant difference in the weights associated with basis 1
217 between the two groups (Fig. 2B), which suggests a link between rhamnolipid production and
218 bacterial growth. To pinpoint features associated with rhamnolipid production, we divided
219 each growth curve into three phases based on its shape (Fig. 2C and Supplementary Fig. 4)
220 and defined 7 quantitative features to characterize each growth phase (Fig. 2D and
221 Supplementary File 2). Using Random Forest classification, we found that the top two
222 features with the highest explanatory power were the maximum and averaged specific growth
223 rates in phase I when growth speeds up (Fig. 2E). Considering the majority of rhamnolipids
224 are produced in phase II when growth slows down (Boyle *et al*, 2015), our finding revealed a
225 strong temporal link between exponential growth rate in phase I and rhamnolipid production
226 in phase II. We hypothesized that the link might be mediated by metabolic homeostasis: its
227 disruption could slow down exponential growth in phase I and disfavor rhamnolipid secretion

228 in phase II by saving precious carbon resources for cell maintenance and stress responses
229 under metabolic imbalanced conditions.

230 **Rhamnolipid non-producers have perturbed TCA cycle and amino acid pathways.**
231 Similar to our growth curve analysis, we adopted both unsupervised and supervised learning
232 approaches to test the associations of intracellular metabolite levels with swarming and
233 rhamnolipid production. We profiled the intracellular metabolome of all our strains in the
234 same glycerol minimal medium (except for two rhamnolipid non-producers M55212 and
235 F23197 which grew too slow) during the transition between phase I and phase II when
236 rhamnolipid production begins (**Materials and Methods**). Using LC-MS (Liquid
237 chromatography-Mass spectrometry) we identified a total of 92 compounds spanning a wide
238 range of abundances (Supplementary Fig. 5A), including 67 metabolites whose identities are
239 known and abundances vary significantly across all the tested strains (Fig. 3A). After data
240 normalization and imputation (Supplementary Fig. 5B), hierarchical clustering showed the
241 consistency of data across all three replicates for each strain (Fig. 3B), except for one
242 replicate of H47921 (sample 25, an outlier removed from further analysis). The similarity
243 among the metabolomics data yielded three major clusters with one cluster (middle cluster in
244 Fig. 3B) containing all strong swarmers (strain name in red) and only rhamnolipid producers.
245 However, no clear metabolic pattern was found among non-producers: Two non-producers
246 were grouped in the left cluster and 4 in the right cluster, and they all had metabolomics
247 profiles similar to producers within the same cluster.

248 The lack of a clear metabolomic profile for rhamnolipid non-producers led us to search for
249 specific differential metabolites using supervised methods. We fitted our metabolomic data
250 (explanatory variables) to categorized rhamnolipid production (response variable) using
251 Orthogonal Projections to Latent Structures-Discriminant Analysis (OPLS-DA) (Cloarec *et*

252 *al*, 2005). The OPLS-DA produced a reasonable fit (R^2 = 0.82, Q^2 = 0.66, *p*-value = 5e-4)
253 with the single predictor that separated rhamnolipid non-producers from producers explaining
254 only 5% of the variance across all data (Fig. 4A). The remaining 95% of the variance was
255 explained by three orthogonal components that capture variation within both groups, again
256 showing that there is a high overlap between the metabolomic profiles of rhamnolipid
257 producers and non-producers. The loading values of the predictive component reflect how
258 much each compound contributes to the separation between rhamnolipid producers and non-
259 producers with negative loadings indicating higher metabolite abundance in non-producers
260 (Fig. 4B and Supplementary Fig. 6).

261 We then used a univariate Mann-Whitney U test to identify the metabolites differentially
262 abundant in producers and non-producers. We found 24 such metabolites (bars with black
263 outline in Supplementary Fig. 6) and these metabolites were then used to identify pathways
264 perturbed in non-producers using the FELLA algorithm (Picart-Armada *et al*, 2017, 2018)
265 (Supplementary Table 1). The most discriminative pathways were the TCA cycle and amino
266 acid metabolism (Fig. 4B). 3 out of 6 metabolites in the TCA cycle—fumarate, succinate and
267 citrate—were significantly changed: Fumarate and malate showed a positive loading value,
268 while citrate, succinate, and to a less extent cis-aconitate and alpha-ketoglutarate were
269 negative (Fig. 4B). Pyruvate remained relatively constant across all the strains (Fig. 3A),
270 implying that the differential responses in the TCA cycle were independent from the changes
271 in its upstream central carbon metabolism.

272 Besides the TCA cycle metabolites, the majority of annotated compounds in the metabolism
273 of branched chain amino acids (leucine/isoleucine, valine) and sulfur-containing amino acids
274 (cysteine/methionine) had higher abundance in rhamnolipid non-producers relative to
275 producers. In fact, with the exception of glutamate, proline and tryptophan, all other amino

276 acids detected in our metabolomics data (threonine, alanine, aspartate, glutamine, cysteine,
277 lysine, histidine, tyrosine, and arginine) were higher in non-producers (Supplementary Fig.
278 6). A striking exception to this trend was formylmethionine (fMet), which had lower
279 abundance in non-producers. Diminished level of fMet had also been found in the Δ*rhlA*
280 mutant of *P. aeruginosa* (Supplementary Fig. 7) (Boyle *et al*, 2017). Since Δ*rhlA* mutant
281 grows with a similar growth rate as the wild-type (van Ditmarsch & Xavier, 2011) the link
282 between fMet and rhamnolipid production should not be simply due to a growth defect.

283 **Metabolome signature and computer simulations link high oxidative stress to lower**
284 **rhamnolipid production.** So far our metabolomics data show that the non-producers have
285 perturbed TCA cycle activity and grow slowly. As shown in Fig. 4C, the TCA cycle harbors
286 five enzymes with Fe-S clusters (aconitase A, aconitase B, succinate dehydrogenase,
287 fumarase A, fumarase B (Py & Barras, 2010)) and thus represents one of the most vulnerable
288 pathways subject to attacks of ROS. It is likely that higher oxidative stress in the non-
289 producers reduces flux through the TCA cycle, which would explain their slower growth. The
290 significantly opposite association of succinate and fumarate we found in rhamnolipid
291 production indicates the reduced activity of succinate dehydrogenase (SDH) under oxidative
292 stress conditions. SDH is a membrane-bound dehydrogenase linked to the respiratory chain—
293 a major site of ROS production in the cell—and also a member of the TCA cycle that
294 catalyzes the oxidation of succinate into fumarate (Hederstedt & Rutberg, 1981). Since SDH
295 contains [2Fe-2S], [3Fe-4S], and [4Fe-4S] clusters (Ayala-Castro *et al*, 2008), ROS that
296 damages Fe-S clusters could decrease SDH activity *in vivo*. The metabolomics data also
297 showed that some intermediate metabolites in amino acid biosynthetic pathways, which are
298 also substrates of Fe-S containing enzymes, accumulated in the non-producers (Fig. 4C). For
299 example, the glutamate synthetase that consists of a large chain (encoded by *gltB*) and a small
300 chain (encoded by *gltD*). Both subunits contain Fe-S clusters and catalyze the production of

301 glutamate from oxoglutarate and glutamine. We found slightly higher oxoglutarate and
302 glutamine as well as lower glutamate in the non-producers. These observations collectively
303 suggest that the rhamnolipid non-producers might have higher oxidative stress levels than the
304 producers.

305 These reasons suggest that the cause for impaired rhamnolipid production might be that non-
306 producing strains suffer from high oxidative stress. We then sought to use a whole-genome
307 reconstruction model to study how oxidative stress could lower the flux of carbon available to
308 rhamnolipid production. We modified a high-quality genome-scale model of *Pseudomonas*
309 metabolism, iJN1411 (Nogales *et al*, 2017, 2020), to simulate growth in the culture medium
310 used in our metabolomics experiments with glycerol and ammonium as the sole carbon and
311 nitrogen sources. Rhamnolipids are produced when carbon is in excess (Boyle *et al*, 2015). In
312 this model rhamnolipids secretion occurs when the carbon-to-nitrogen (C:N) ratio exceeds a
313 6.3 threshold (Supplementary Fig. 8). We set C:N to 10.0, which exceeds the minimum
314 threshold, and we varied the redox stress level by changing the flux levels of three redox
315 molecules: NADH (reduced nicotinamide adenine dinucleotide), NADPH (reduced
316 nicotinamide adenine dinucleotide phosphate) and GSH (reduced glutathione); these
317 molecules are responsible for the bulk of cellular electron transfer and likely to be the main
318 sources of ROS (Xiao & Loscalzo, 2019). Although redox stress is ultimately caused by high
319 ROS levels, not fluxes, and ROS was not an explicit variable in our model, we assumed that
320 ROS can perturb intracellular metabolic fluxes, particularly the fluxes of redox molecules,
321 and asked how cell growth and rhamnolipid secretion respond to these ROS-mediated
322 indirect perturbations.

323 For all three redox molecules, we found that the maximum growth rate was maintained at an
324 intermediate flux range (redox homeostasis, white area) while any flux rate outside the range

325 (gray shading) gradually reduced growth rate (Fig. 5, upper panels). What generally
326 accompanied the compromised growth rate was the abrupt shutdown of secretion of
327 rhamnolipid precursors (HAA), mono- and di-rhamnolipids as well as many (but not all)
328 central carbon metabolites, except for extremely small GSH flux (Fig. 5, lower panels).
329 Importantly, reducing any of these secretion fluxes did not reduce the growth rate, nor did it
330 provide growth benefits (i.e., each individual flux could be as low as zero without reducing
331 maximum growth rate). This observation agrees with the data that the *ΔrhlA* mutant of *P.*
332 *aeruginosa* type strain PA14 has the same grow rate as its wild-type strain in the same
333 glycerol minimal medium (van Ditmarsch & Xavier, 2011). Notably, most of the overflowed
334 carbon-rich molecules, including HAA, mono- and di-rhamnolipids, were only secreted when
335 the growth rate maintained its maximum value under excess carbon. The computational
336 inference that rhamnolipids, as well as other central carbon metabolism intermediates, can be
337 secreted under maximum growth suggests that *P. aeruginosa* cells have the flexibility to
338 overflow carbon through alternative metabolic pathways without compromising growth. The
339 fact that *P. aeruginosa* maintains the secretion of rhamnolipids among these options supports
340 that rhamnolipid secretion was favored by natural selection for reasons other than improving
341 single-cell fitness. Collectively, these simulations support a link between rhamnolipids
342 secretion and redox stress, where fast growth and rhamnolipid secretion are both
343 metabolically constrained by cellular redox homeostasis.

344 **Experiments support the link between growth, oxidative stress and rhamnolipid**
345 **production.** We validated the link between oxidative stress and rhamnolipid production by
346 two additional experiments. In the first experiment, we monitored growth and rhamnolipid
347 production of all our clinical isolates when they grew in the same minimal medium but with
348 succinate as the sole carbon source (Supplementary Fig. 9). Since succinate enters the carbon
349 metabolism directly through the TCA cycle, we expected that, compared to growth in

350 glycerol, the initial TCA cycle flux would be much faster and generates higher ROS level that
351 impairs the sustained cell growth and rhamnolipid secretion. Indeed, none of the strains that
352 produced rhamnolipids in glycerol produced rhamnolipids in succinate. We similarly
353 extracted 7 phase-dependent growth curve features of our strains grown in succinate
354 (Supplementary File 3) and compared their values to the same features measured in glycerol
355 (Supplementary Fig. 10). The comparison showed that all strains had shorter lag phases and
356 grew exponentially faster in succinate. The strains reached much lower cell densities even
357 though the succinate medium had the same initial molar concentration of carbon as the
358 glycerol medium. More interestingly, phase II was almost absent in succinate compared to
359 glycerol. The strains all switched abruptly from phase I to phase III, suggesting that cells
360 might have accumulated more oxidative stress during phase I, which caused a sudden stop in
361 growth as well as carbon overflow.

362 In the second experiment, we monitored the hydrogen peroxide (H_2O_2) level when growing
363 our *Pseudomonas* strains in the glycerol minimal medium (Fig. 6A,B). H_2O_2 is a
364 representative ROS that can diffuse freely between cell and the environment. By measuring
365 the fluorescent signal intensity produced by the Amplex assay (**Materials and Methods**), we
366 found a baseline production of H_2O_2 in the absence of cells, possibly due to photooxidation of
367 Amplex Red reagent (Zhao *et al*, 2012). When cells were added, *Pseudomonas* strains can
368 degrade H_2O_2 by producing many antioxidant enzymes including catalases, glutathione
369 reductase, NADH peroxidase and cysteine-based peroxidases (Mishra & Imlay, 2012). We
370 computed the signal intensity difference between cell culture and baseline as a proxy of the
371 ability of each strain to remove H_2O_2 and broadly combat oxidative stress. We saw that all
372 strains except for M1608 quenched the signal over the first 18 hours (Fig. 6B). Most
373 importantly, the non-producers (blue lines) removed less H_2O_2 than mild rhamnolipid
374 producers (green lines) and strong producers (red lines), supporting our hypothesis that non-

375 producers are worse at removing ROS. Unsurprisingly, the worst strain in this assay was
376 M1608, which lacks *katE* and *gor* (Table 1), both of which are important for H_2O_2
377 degradation. To factor out the possibility that the non-producers performed worse due to
378 lower cell density, we calculated the H_2O_2 removal rate per cell and observed similar relative
379 trend of H_2O_2 degradation between non-producers and producers (Fig. 6C). Formally, we
380 used a linear mixed-effect model to test the effect of rhamnolipid production on per-cell H_2O_2
381 removal rate (**Materials and Methods**). The effect size of mild and strong producers relative
382 to the non-produces are 1.25x and 1.41x stronger respectively with both p-values < 0.001,
383 confirming that rhamnolipid producers deal better with oxidative stress.

384 Discussion

385 Our data comparing growth phenotypes and metabolomes posit a model to explain the
386 diversity of swarming phenotypes we saw in *P. aeruginosa* isolates (Fig. 7): Some strains can
387 produce rhamnolipids because they maintain redox homeostasis due to their greater abilities
388 to degrade ROS. Rhamnolipid non-producers by contrast had disrupted redox homeostasis,
389 causing slower growth with reduced TCA cycle activity and increased amino acid
390 concentration. The impaired ability to degrade ROS by non-producers is possibly caused by
391 loss of genes that encode ROS detoxification functions (e.g., M1608 lacks *katE* and *gor*).
392 Consistently, it was reported that OxyR—oxidative stress regulator that controls expression
393 of antioxidant genes—is required for swarming and rhamnolipid production (Vinckx *et al*,
394 2010).

395 All our clinical strains were isolated from hospitalized patients, a host-associated
396 environment where we may expect redox stresses such as ROS imposed by the immune
397 system in their fight against pathogens (Puertollano *et al*, 2011) and by antibiotics treatment
398 (Zhu *et al*, 2019). Non-producers of rhamnolipids seem less capable of dealing with oxidative

399 stresses, and it remains unclear what selected for this loss of function *in vivo*. Rhamnolipid
400 production was, nonetheless, relatively frequent across the *P. aeruginosa* phylogenetic tree.
401 The genes for rhamnolipid biosynthesis (*rhlA*, *rhlB*, *rhlC*) remained intact across all of our
402 clinical isolations, even in non-producers. This suggests that the loss of rhamnolipid
403 production in some strains may have resulted from broader metabolic adaptations such as
404 oxidative stress responses. In support of our model we saw that rhamnolipid producers could
405 quench oxidation faster than non-producers (Fig. 6). Accumulation of oxidative stress due to
406 slow removal can reduce SDH activity and perturb TCA cycle (Fig. 7). Others have shown
407 that *P. aeruginosa* decreases expression of the key quorum-sensing genes (*LasI*, *LasR*, *RhlI*,
408 *RhlR*, *PqsA* and PqsR) in response to oxidative stress caused by exposure to H_2O_2 (Mohamed
409 *et al*, 2020). Considering quorum sensing regulates hundreds of genes (Lequette *et al*, 2006),
410 shutting down the cooperative traits that are under quorum-sensing regulation—including
411 rhamnolipid secretion—could save precious resources for oxidative stress responses.

412 We also saw that rhamnolipid non-producers had significantly lower levels of fMet than
413 producers. Interestingly, this also happens in the Δ*rhlA* mutant compared to its wild-type
414 strain PA14 (Boyle *et al*, 2017). fMet plays a role in translation initiation, and in the quality
415 control mechanisms that degrade misfolded proteins (Piatkov *et al*, 2015). *Bacillus subtills*
416 lacking Formyl-Methionine Transferase (FMT)—the enzyme attaching a formyl group to
417 methionine loaded on $tRNA^{fmet}$—are more sensitive to H_2O_2 and defective in swarming (Cai
418 *et al*, 2017). The link between fMet, swarming and oxidative stress is intriguing and warrants
419 further research.

420 Only the strains that grew fast on glycerol could produce rhamnolipids in that medium. This
421 supports the notion that rhamnolipid production is a form of overflow metabolism. Overflow
422 metabolism is associated with fast growth such as bacteria under conditions of high glucose

423 consumption. It occurs when cells simultaneously operate on both energy-efficient (e.g.,
424 respiration) and -inefficient (e.g., fermentation) pathways and secret metabolic byproducts
425 that could otherwise be used for catabolism or anabolism. This phenomenon has been
426 observed in different systems: aerobic fermentation in *Escherichia coli* (Farmer & Jones,
427 1976), the Crabtree effect in *Saccharomyces cerevisiae* (De Deken, 1966) and the Warburg
428 effect in cancer cells (Vander Heiden *et al*, 2009). Many molecular mechanisms have been
429 proposed and validated to account for the seemingly wasteful usage of low energy-yield
430 pathway in presence of a higher-energy-yield alternative (Basan *et al*, 2015; Szenk *et al*,
431 2017). For example, the respiratory flux that would be required for fast growth without
432 fermentation could accumulate NADH that could not be recycled to NAD^+ by respiration
433 alone, because of a limited surface/volume ratio (Szenk *et al*, 2017). Overexpression of
434 NADH oxidase in both *E. coli* (Vemuri *et al*, 2006) and *S. cerevisiae* (Vemuri *et al*, 2007)
435 reduced the $NADH/NAD^+$ ratio and suppressed overflow metabolism. One key difference
436 between *P. aeruginosa* rhamnolipid production and the overflow metabolism of other
437 systems is that rhamnolipids are controlled by quorum-sensing in addition to nutrient cues
438 (Boyle *et al*, 2015), which results in a cell-density-dependence.

439 Should rhamnolipid production provide a fitness benefit for *P. aeruginosa* under any
440 environmental conditions? We have previously shown that rhamnolipid production is
441 dispensable for normal growth of *P. aeruginosa* in laboratory conditions: the Δ*rhlA* mutant is
442 an engineered rhamnolipid non-producer defector but has almost the same growth rate (van
443 Ditmarsch & Xavier, 2011) and very similar metabolomic profiles (Boyle *et al*, 2017) as the
444 wild-type. This is consistent with our flux-balance analysis of *Pseudomonas* metabolism,
445 where shutting down rhamnolipid secretion did not impact the growth rate because the excess
446 carbon could be alternatively secreted in other forms such as acetate (Fig. 5). Notably, Δ*rhlA*
447 had higher intracellular levels of gamma-Glutamylcysteine (Supplementary Fig. 7), the

448 immediate precursor of glutathione. Since glutathione is a well-known antioxidant that
449 protects cells from ROS damage (Ezraty *et al*, 2017), Δ*rhlA* may exhibit slight oxidative
450 burden. This could explain why the Δ*rhlA* has a marginally lower fitness and fails to invade
451 the wild-type in swarming competitions (de Vargas Roditi *et al*, 2013; Monaco *et al*, 2020).
452 Our mechanism proposes that increased oxidative burden may be related to altered redox
453 ratio (NAD(P)H/NAD(P)$^+$), considering that fatty acid biosynthesis that provides precursors
454 for rhamnolipid production regenerates NAD(P)+ from NAD(P)H. Notably, the active
455 shutdown of rhamnolipid production in redox imbalanced condition would save precious
456 carbon and enzyme resources to respond to oxidative stress.

457 Our results confirm the role that metabolic byproducts play in linking single-cell physiology
458 and social behavior. Microorganisms secrete various products, including iron scavenging
459 siderophores (Griffin *et al*, 2004), extracellular enzymes (Altindis *et al*, 2015), toxins and
460 cell-cell signaling molecules (Schmidt *et al*, 2019). In synthetic and natural microbial
461 communities the products of one microorganism can impact another, cooperatively or
462 competitively (Xavier, 2011). Our model proposes that the choice of a given molecule to
463 drive a social interaction is not arbitrary: molecules that conciliate individual-level and
464 population-level interests are more likely to drive microbial sociobiology.

465 Materials and Methods

466 **Media.** Glycerol and succinate synthetic media were prepared with 800 ml of Milipore water,
467 200 ml of 5X minimal salts buffer, 1ml of 1 M magnesium sulphate, 0.1 ml of calcium
468 sulphate with 0.5 gN/l nitrogen (ammonium sulphate), iron at 5 μM (iron III sulphate) and 3.0
469 gC/l glycerol or succinate, respectively. Swarming agar consisted in 800ml of Milipore water,
470 200 ml of 5X minimal salts buffer, 1ml of 1 M magnesium sulphate, 0.1 ml of calcium
471 sulphate, 25 ml of 200 g/l solution of casamino acids (Bacto TM from BD, Sparks,MD) with

472 0.5% of agar. 5X stock minimal salts buffer was prepared with 12 g of Na_2HPO4
473 (anhydrous), 15 g of KH_2PO4 (anhydrous) and 2.5 g of NaCl into 1 l water.

474 **Succinate and glycerol growth curve assays.** The clinical isolates were inoculated in 3 mL
475 of lysogen broth (LB) and incubated at 37ºC overnight with shaking at 250 rpm. 500 µL of
476 cell culture was pelleted and washed 3 times with PBS. 0.0025 OD_{600} units were inoculated
477 into 3.0 gC/l glycerol or succinate minimal medium in BD Falcon (BD Biosciences, San Jose,
478 CA) 96 well flat-bottom plates, with 150 µL of suspension per well. The plate was incubated
479 during 48 hours at 37ºC in a Tecan Infinite M1000 or Tecan Infinite M1000 Pro plate reader
480 (Männedorf, Switzerland), with an orbital shaking of 4 mm of amplitude. OD_{600} was
481 measured in 10 minutes intervals.

482 **Swarming assay** Swarming assays were performed as described previously (Xavier *et al*,
483 2011; van Ditmarsch *et al*, 2013). The clinical isolates were inoculated in 3 mL of LB and
484 incubated at 37ºC overnight, with shaking. 500 µL of the culture was pelleted and washed
485 twice with PBS. 2 µL of this suspension was spotted on the surface of swarming agar without
486 penetrating the agar with the pipette tip. Swarming medium contains 0.5% agar (Bacto) and is
487 supplemented with 5g/L casamino acids, 1mM MgSO4, 0.1mM CaCl2 and 1X salt buffer
488 (12g/L Na_2HPO_4 (Fisher Scientific), 15g/L KH_2PO4 (Fisher Scientific) and 2.5g/L NaCl,
489 pH6.7). The plates were incubated at 37ºC ~24 hours. Two replicates were done per strain. In
490 each batch of swarming assays PA14 was used as control.

491 **Rhamnolipid production quantification.** The production of rhamnolipids was assessed by
492 drop-collapse assay (Jain & Collins; Chen *et al*, 2007). We placed 50 µL of the culture's
493 supernatant on a polystyrene surface (the lid of a 96 well plate). The presence of
494 rhamnolipids decreases the surface tension of the liquid, making the drop collapse. We
495 considered a strain rhamnolipid non-producer if the drop does not spread, a mild-producer if

496 spreads, but not enough to pass over the lid's circle that correspond to the wells, and producer
497 if spreads over it.

498 **Image analysis and quantification of swarming phenotype.** Images of the swarming plates
499 were obtained with a Chemidoc gel doc imager (Bio Rad). The extraction of the
500 morphological features from the images of the swarming plates were analyzed using Matlab
501 bwmorph function. The features extracted from the images were perimeter of the colony,
502 maximum length (the longitude of the rectangle that fits the colony), area percentage of the
503 plate occupied by the colony, circularity (measured as $4*\pi/P^2$, where P is the perimeter of the
504 colony), longitude of the skeleton (skeletonization, consisting in all the points that are at
505 equal distance to their nearby borders) and eccentricity (the eccentricity of the fitted ellipse).
506 The feature values of each strain were normalized by the corresponding values of the PA14
507 strain in the same experiment. The swarming score (S_i) for each clinical isolate i is defined as
508 a linear combination of the maximum length (L_i) and circularity (C_i) of its swarming colony
509 (the two most discriminative features that separate strong swarmers from weak swarmers; see
510 Supplementary Fig. 1)

$$S_i = 0.60(L_i - \tilde{L}) - 0.80(C_i - \tilde{C}) \quad (1)$$

511 where $\tilde{L}$ and $\tilde{C}$ are the mean values of L_i and C_i across all clinical isolates respectively, and
512 the linear coefficients maximize the variance of the swarming score. To binarize the
513 swarming phenotype, a strain is called swarmer if its swarming score is higher than the
514 median swarming score across all strains (otherwise it is a non-swarmer).

515 **Cross-strain reciprocal BLAST.** To identify orthologous gene across all *P. aeruginosa*
516 strains, systematic cross-strain reciprocal BLAST was performed. Protein sequences of each
517 strain and the type strain PA14 were mutually queried against and the BLAST hits (genes)

518 with <80% coverage were removed. Two genes are orthologous if they were mutually the
519 best hit to each other and genes (from other strains) that are orthologous to the same PA14
520 gene were considered orthologous to each other.

521 **Phylogenetic analysis.** The phylogenetic tree of clinical *P. aeruginosa* strains (Fig. 1A) was
522 constructed from core genomes as previously described (Yan *et al*, 2017). Moran's I test was
523 carried out using the ape package in R (Paradis & Schliep, 2019). The ancestral state of
524 swarming and rhamnolipid production was reconstructed using corHMM package (Beaulieu
525 *et al*, 2013).

526 **Growth curve analysis.** We first normalized the growth curves in different experiments
527 (plates) by matching their corresponding controls (PA14). The plate-specific coefficients
528 were obtained by solving a linear regression model 'log(OD of PA14) ~ Plate + Time' (the
529 Wilkinson notation) using Matlab function fitlm, where Plate is plate ids and Time is time
530 points (both are categorical variables). Then the growth curves in each plate were normalized
531 by multiplying the adjustment coefficient of the plate. These normalized growth curves were
532 then smoothed by Savitzky-Golay filter (sgolayfilt function in Matlab). The growth phases
533 (phase I, II, III) were determined by the following rules: (phase I): first-order derivative >0
534 and second-order derivative >0; (phase II) first-order derivative >0 and second-order
535 derivative <0; (phase III) first-order derivative <0. The mean and maximum specific growth
536 rate for each growth phase were estimated from the best-fit model (highest R2) among three
537 models of bacterial growth curves: (1) exponential model $y = y_0 + y_1 e^{\mu t}$; (2) Zwietering-
538 Logistic model $y = y_0 + (A - y_0)\left(1 + e^{\frac{4\mu}{A}(\lambda - t) + 2}\right)^{-1}$; (3) Zwietering-Gompertz model
539 $y = y_0 + (A - y_0)e^{-e^{\frac{\mu e}{A}(\lambda - t) + 1}}$, where $y_0, y_1, \mu, \lambda, A$ are the parameters to fit. Both non-
540 negative factorization and random forest regression were performed in python, by
541 sklearn.decomposition.NMF and sklean.ensemble.RandomForestClassifier respectively.

542 **Metabolite extraction.** All *P. aeruginosa* strains were grown until OD_{600} = 0.2 (end of
543 exponential phase of growth) in glycerol minimal media. Bacteria was then loaded into 0.25
544 µm nylon membranes (Millipore) using vacuum, transferred to pre-warmed hard agar plates
545 with the same medium composition and incubated at 37ºC during 2.5 h. The filters were then
546 passed to 35 mm polystyrene dishes (Falcon) with 1 mL of 2:2:1 methanol:acetonitrile:H_2O
547 quenching buffer and incubated there during 15 minutes on dry ice. Cells were removed by
548 scraping and the lysate containing quenching buffer was transferred to 1.5 mL tubes and
549 centrifuged at 16000 rpm for 10 minutes at 4ºC. Supernatant transferred to fresh tubes and
550 stored at -80ºC.

551 **Metabolomic data preprocessing.** The extracts were profiled using liquid-chromatography
552 coupled to mass spectrometry (LC-MS), identifying a total of 92 compounds (Supplementary
553 Fig. 5). Some compounds contained missing values. These missing values in metabolite
554 abundance can be (1) truly missing; (2) present in a sample but its level is below detection
555 limit; (3) present in a sample at a level above the detection limit but missing due to failure of
556 algorithms in data processing. Here we assume that a metabolite with missing values in all
557 three replicates is truly missing in the sample and removed from our analysis (Supplementary
558 Fig. 5). However, if the missing values were only found in one or two replicates, the missing
559 values were imputed by the average of the non-missing values. After that imputation all
560 compounds with missing values were removed (Supplementary Fig. 5).

561 The peak areas were normalized using Cross-Contribution Compensating Multiple Standard
562 Normalization (CCMN) (Redestig *et al*, 2009) with NormalizeMets R package (De Livera *et*
563 *al*, 2018). This method relies on the use of multiple internal standards. Since LC-MS lacks
564 such internal standards, we used instead a set of metabolites assumed to be constant across all
565 the strains. They were selected with a Kuskal-Wallis test, adjusting the *p*-value with

566 Benjamini-Hochberg method. The ones with a *p*-value above 0.05 were considered constant
567 (pyruvate, methylglyoxal, (S)-2-Acetolactate, Tyramine, D-Glucose, (S)-Lactate, N-acetyl-L-
568 glutamate 5-semialdehyde, 4-Aminobutyraldehyde and Glycine), therefore after the
569 normalization step they were removed (indicated in red, Fig. 3A).

570 **Hierarchical clustering of metabolomic data.** The hierarchical clustering of the normalized
571 metabolomic data (Fig. 3B) was performed using gplots R package (Warnes *et al.* 2009), with
572 Euclidean distance and Ward's aggregation method. The clustering was performed with all
573 metabolites; however, 16 metabolites (indicated in red, Fig. 3A) with unknown compound
574 identity were removed from Fig. 3B and downstream analyses. These unknown compounds
575 are not artifacts arising from LC-MS instruments since their peaks were detected in all
576 strains. Fumarate and guanosine, which were only putative initially, were bioinformatically
577 confirmed as all other compounds with the same molecular weight are produced by
578 enzymatic reactions missing in our clinical isolates.

579 **Metabolic pathway enrichment.** The differential metabolites between rhamnolipid
580 producers and non-producers was determined by a Mann-Whitney test, with *p*-values
581 adjusted with Benjamini-Hochberg method and a significance level of 0.05. These
582 compounds were fed to FELLA algorithm (Picart-Armada *et al*, 2018, 2017). FELLA
583 retrieves a graph describing the relationships among pathway, module, enzyme, reaction and
584 compounds of *Pseudomonas aeruginosa* strain UCBPP-PA14 from the KEGG database. The
585 graph was then used as an input network of differential compounds for its diffusion
586 algorithms (Vandin *et al* 2011). The output of FELLA consists of all subnetworks of the
587 entries predicted to have a high connectivity with the differential compounds. We filtered the
588 subnetwork entries to keep only metabolic pathways.

589 **OPLS-DA model.** OPLS-DA model of metabolomics data was built using ropls R package
590 (Thévenot *et al*, 2015), fixing the number of orthogonal components to 3. R^2 and Q^2, key
591 parameters for assessing the validity of the model, were assessed with 7-fold cross validation.
592 The significance of the model was determined by permutation test (n = 2000). The *p*-value
593 corresponds to the proportion of Q^2_{perm} above Q^2. With a *p*-value below 0.05 we considered
594 the model significant. The loadings of the predictive component of the model were extracted
595 to determine how each metabolite contributes to the separation according to the phenotype.

596 **Genome-scale modeling.** Custom Python codes were developed with the COBRApy
597 package (Ebrahim *et al*, 2013) to carry out all metabolic flux modeling and simulations in the
598 paper. Since iJN1411 model was developed for *Pseudomonas putida*, we removed genes and
599 associated reactions that are missing in all our strains but present in the iJN1411 model. The
600 futile cycles involving NADH, NADPH, and GSH were also removed. The modified iJN1411
601 model was further expanded by adding rhamnolipid biosynthesis pathway involving 9 new
602 metabolites and 12 new reactions. The metabolites, reactions and genes of the final model are
603 given in JSON format (Supplementary File 4).

604 The boundary fluxes of the model were set to mimic the composition of the glycerol
605 minimum medium. For C:N=10, the lower bounds of glycerol and ammonium fluxes were set
606 to -10 and -3 respectively. For C:N=3, the lower bounds were set to -3 and -3 respectively.
607 The flux unit is mmol/gDW/h throughout the paper. To constrain the total producing flux of
608 NADH (the same for NADPH and GSH) at a certain value C, we first defined a binary
609 variable X_k for each NADH-involving reaction k to indicate whether NADH is produced by
610 this reaction. Given the stoichiometric coefficient of NADH in this reaction (s_k) and its flux
611 value (f_k), the mathematical constraints for X_k was set by $X_k = 1$ for $s_k f_k > 0$ and $X_k = 0$
612 otherwise. Therefore, the constraint that equalizes the total NADH producing flux and a

613 constant C is simply $\sum_k s_k X_k f_k = C$. However, both X_k and f_k are variables and such
614 quadratic constraint has not yet been supported by COBRApy. We overcame this difficulty
615 by defining $A_k = X_k f_k$ and linearized the product with the following two inequalities:
616 $X_k l_b \leq A_k \leq X_k u_b$ and $f_k - (1 - X_k)u_b \leq A_k \leq f_k - (1 - X_k)l_b$, where l_b and u_b are the
617 lower and upper bounds of f_k. The two constraints ensure that $A_k = 0$ when $X_k = 0$ and
618 $A_k = f_k$ when $X_k = 1$. The minimum/maximum flux values of byproduct secretion were
619 simulated by flux variability analysis at maximum growth rate.

620 **Detection of hydrogen peroxide (H_2O_2)**. The H_2O_2 level in the extracellular medium was
621 quantified with Amplex® Red Hydrogen Peroxide/Peroxidase Assay Kit (Invitrogen,
622 Carlsbad, USA, Catalog no. A22188). 500 µL of cell suspension were spinned down after
623 overnight growth in LB medium, washed twice in PBS and normalized to OD 1. Each
624 reaction was done in a final volume of 100 µL, with a final concentration of 50 µM of
625 Amplex® Red reagent, 0.1 U/mL of HRP (Horseradish Peroxidase) and 0.2 cell OD, in
626 glycerol synthetic medium, in BD Falcon (BD Biosciences, San Jose, CA) 96 well flat-
627 bottom plates. The first column of the plate corresponded to the reaction without cells (the
628 volume was substituted by PBS), and the last column instead of cells contained H_2O_2 (final
629 concentration 10 µM). OD_{600} and fluorescence 530/590 nm was measured in 10 minutes
630 intervals (48 h 37ºC).

631 **Hydrogen peroxide (H_2O_2) degradation.** H_2O_2 was removed from environment by cells
632 which degrade H_2O_2 intracellularly. The cumulative H_2O_2 removal curve was calculated by
633 subtracting the values of emission of the wells containing each strain from the values of
634 emission of the wells without cells or H_2O_2. Then they were normalized to the relative scale
635 by dividing their values by the corresponding values (at the same time points) of the control
636 strain (PA14) in the same experiment (plate). These normalized curves were then smoothed

637 by the Savitzky-Golay filter (sgolayfilt function in Matlab). The H_2O_2 removal rate per cell
638 was calculated by dividing the first-order derivative of the cumulative removal curves by OD
639 values. To estimate the effect of rhamnolipid production on per-cell H_2O_2 removal rate, we
640 developed a linear mixed-effect model that extends the simple linear regression model by
641 considering both fixed and random effects. The model was specified by the Wilkinson
642 notation 'RemovalRate ~ Time + RHL + (1|CurveID)', where RemovalRate is per-cell H_2O_2
643 removal rate, Time is time point (categorical variable), RHL is categorical rhamnolipid
644 production (non-producer, mild-producer, and strong-producer), and CurveID is the unique
645 ID for each strain and replicate. The expression '(1|CurveID)' indicates that CurveID was
646 modeled as random effects. The model was solved by fitlme in Matlab.

647

648 **Data availability**

649 All experimental and simulation data that support the conclusions of this study are available
650 from the main text and Supplementary Information. The source codes for generating the
651 figures of this study are available from
652 https://github.com/liaochen1988/Source_code_for_Pseudomonas_Metabolomics_Paper.

653 **Acknowledgements**

654 This work was supported by NIH grants U01 AI124275 and R01 AI137269-01 to J.B.X.
655 F.R.P. and G.S. were partially supported by UIDB/04046/2020 and UIDP/04046/2020 Centre
656 grants from FCT, Portugal (to BioISI) and by the LungCARD project (Grant Agreement nº:
657 734790, H2020-MSCA-RISE-2016). G.S. is recipient of a fellowship from BioSys PhD
658 programme PD65-2012 (Ref SFRH/BD/142899/2018) from FCT (Portugal). The funders had

659 no role in study design, data collection and analysis, decision to publish, or preparation of the
660 manuscript.
661

662 **References**

663 Abdel-Mawgoud AM, Lépine F & Déziel E (2010) Rhamnolipids: diversity of structures,
664 microbial origins and roles. *Appl. Microbiol. Biotechnol.* **86:** 1323–1336
665 Altindis E, Dong T, Catalano C & Mekalanos J (2015) Secretome analysis of *Vibrio cholerae*
666 type VI secretion system reveals a new effector-immunity pair. *MBio* **6:** e00075
667 Ayala-Castro C, Saini A & Outten FW (2008) Fe-S cluster assembly pathways in bacteria.
668 *Microbiol. Mol. Biol. Rev.* **72:** 110–25, table of contents
669 Basan M, Hui S, Okano H, Zhang Z, Shen Y, Williamson JR & Hwa T (2015) Overflow
670 metabolism in *Escherichia coli* results from efficient proteome allocation. *Nature*
671 **528:** 99–104
672 Beaulieu JM, O'Meara BC & Donoghue MJ (2013) Identifying hidden rate changes in the
673 evolution of a binary morphological character: the evolution of plant habit in
674 campanulid angiosperms. *Syst. Biol.* **62:** 725–737
675 Biro PA & Stamps JA (2010) Do consistent individual differences in metabolic rate promote
676 consistent individual differences in behavior? *Trends Ecol. Evol. (Amst.)* **25:** 653–659
677 Boyle KE, Monaco H, van Ditmarsch D, Deforet M & Xavier JB (2015) Integration of
678 metabolic and quorum sensing signals governing the decision to cooperate in a
679 bacterial social trait. *PLoS Comput. Biol.* **11:** e1004279
680 Boyle KE, Monaco HT, Deforet M, Yan J, Wang Z, Rhee K & Xavier JB (2017) Metabolism
681 and the evolution of social behavior. *Mol. Biol. Evol.* **34:** 2367–2379
682 Cai Y, Chandrangsu P, Gaballa A & Helmann JD (2017) Lack of formylated methionyl-

683 tRNA has pleiotropic effects on *Bacillus subtilis*. *Microbiology (Reading, Engl.)* **163:**
684 185–196
685 Caiazza NC, Shanks RMQ & O'Toole GA (2005) Rhamnolipids modulate swarming motility
686 patterns of *Pseudomonas aeruginosa*. *J. Bacteriol.* **187:** 7351–7361
687 Chen CY, Baker SC & Darton RC (2007) The application of a high throughput analysis
688 method for the screening of potential biosurfactants from natural sources. *J.*
689 *Microbiol. Methods*
690 Chong H & Li Q (2017) Microbial production of rhamnolipids: opportunities, challenges and
691 strategies. *Microb. Cell Fact.* **16:** 137
692 Cloarec O, Dumas M-E, Craig A, Barton RH, Trygg J, Hudson J, Blancher C, Gauguier D,
693 Lindon JC, Holmes E & Nicholson J (2005) Statistical total correlation spectroscopy:
694 an exploratory approach for latent biomarker identification from metabolic 1H NMR
695 data sets. *Anal. Chem.* **77:** 1282–1289
696 De Deken R (1966) The Crabtree Effect: A Regulatory System in Yeast. *J. Gen. Microbiol.*
697 **44:** 149–156
698 De Livera AM, Olshansky G, Simpson JA & Creek DJ (2018) NormalizeMets: assessing,
699 selecting and implementing statistical methods for normalizing metabolomics data.
700 *Metabolomics* **14:** 54
701 Deforet M, van Ditmarsch D, Carmona-Fontaine C & Xavier JB (2014) Hyperswarming
702 adaptations in a bacterium improve collective motility without enhancing single cell
703 motility. *Soft Matter* **10:** 2405–2413
704 Déziel E, Lépine F, Milot S & Villemur R (2003) *rhlA* is required for the production of a
705 novel biosurfactant promoting swarming motility in *Pseudomonas aeruginosa*: 3-(3-
706 hydroxyalkanoyloxy)alkanoic acids (HAAs), the precursors of rhamnolipids.
707 *Microbiology (Reading, Engl.)* **149:** 2005–2013

708 van Ditmarsch D, Boyle KE, Sakhtah H, Oyler JE, Nadell CD, Déziel É, Dietrich LEP &
709 Xavier JB (2013) Convergent evolution of hyperswarming leads to impaired biofilm
710 formation in pathogenic bacteria. *Cell Rep.* **4:** 697–708
711 van Ditmarsch D & Xavier JB (2011) High-resolution time series of *Pseudomonas*
712 *aeruginosa* gene expression and rhamnolipid secretion through growth curve
713 synchronization. *BMC Microbiol.* **11:** 140
714 Ebrahim A, Lerman JA, Palsson BO & Hyduke DR (2013) COBRApy: COnstraints-Based
715 Reconstruction and Analysis for Python. *BMC Syst. Biol.* **7:** 74
716 Ezraty B, Gennaris A, Barras F & Collet J-F (2017) Oxidative stress, protein damage and
717 repair in bacteria. *Nat. Rev. Microbiol.* **15:** 385–396
718 Farmer IS & Jones CW (1976) The energetics of *Escherichia coli* during aerobic growth in
719 continuous culture. *Eur. J. Biochem.* **67:** 115–122
720 Griffin AS, West SA & Buckling A (2004) Cooperation and competition in pathogenic
721 bacteria. *Nature* **430:** 1024–1027
722 Hederstedt L & Rutberg L (1981) Succinate dehydrogenase--a comparative review.
723 *Microbiol Rev* **45:** 542–555
724 Inoue T, Shingaki R, Hirose S, Waki K, Mori H & Fukui K (2007) Genome-wide screening
725 of genes required for swarming motility in *Escherichia coli* K-12. *J. Bacteriol.* **189:**
726 950–957
727 Jain DK & Collins DL A drop-collapsing test for screening surfactant-producing
728 microorganisms. *Thompson*
729 Kamatkar NG & Shrout JD (2011) Surface hardness impairment of quorum sensing and
730 swarming for *Pseudomonas aeruginosa. PLoS One* **6:** e20888
731 Kearns DB (2010) A field guide to bacterial swarming motility. *Nat. Rev. Microbiol.* **8:** 634–
732 644

733 Kim W & Surette MG (2004) Metabolic differentiation in actively swarming *Salmonella*.
734 *Mol. Microbiol.* **54:** 702–714
735 Klevens RM, Edwards JR, Richards CL, Horan TC, Gaynes RP, Pollock DA & Cardo DM
736 (2007) Estimating health care-associated infections and deaths in U.S. hospitals, 2002.
737 *Public Health Rep.* **122:** 160–166
738 Köhler T, Curty LK, Barja F, van Delden C & Pechère JC (2000) Swarming of *Pseudomonas*
739 *aeruginosa* is dependent on cell-to-cell signaling and requires flagella and pili. *J.*
740 *Bacteriol.* **182:** 5990–5996
741 Kollaran AM, Joge S, Kotian HS, Badal D, Prakash D, Mishra A, Varma M & Singh V
742 (2019) Context-Specific Requirement of Forty-Four Two-Component Loci in
743 *Pseudomonas aeruginosa* Swarming. *iScience* **13:** 305–317
744 Lee DD & Seung HS (1999) Learning the parts of objects by non-negative matrix
745 factorization. *Nature* **401:** 788–791
746 Lequette Y, Lee J-H, Ledgham F, Lazdunski A & Greenberg EP (2006) A distinct QscR
747 regulon in the *Pseudomonas aeruginosa* quorum-sensing circuit. *J. Bacteriol.* **188:**
748 3365–3370
749 Luo Y, Zhao K, Baker AE, Kuchma SL, Coggan KA, Wolfgang MC, Wong GC & O'Toole
750 GA (2015) A hierarchical cascade of second messengers regulates *Pseudomonas*
751 *aeruginosa* surface behaviors. *MBio* **6:**
752 Mattingly AE, Kamatkar NG, Borlee BR & Shrout JD (2018) Multiple Environmental
753 Factors Influence the Importance of the Phosphodiesterase DipA upon *Pseudomonas*
754 *aeruginosa* Swarming. *Appl. Environ. Microbiol.* **84:**
755 Medina G, Juárez K, Valderrama B & Soberón-Chávez G (2003) Mechanism of
756 *Pseudomonas aeruginosa* RhlR transcriptional regulation of the *rhlAB* promoter. *J.*
757 *Bacteriol.* **185:** 5976–5983

758 Mellbye B & Schuster M (2014) Physiological framework for the regulation of quorum
759 sensing-dependent public goods in *Pseudomonas aeruginosa. J. Bacteriol.* **196:**
760 1155–1164
761 Mishra S & Imlay J (2012) Why do bacteria use so many enzymes to scavenge hydrogen
762 peroxide? *Arch. Biochem. Biophys.* **525:** 145–160
763 Mohamed FA, Shaker GH & Askoura MM (2020) Oxidative Stress Influences *Pseudomonas*
764 *aeruginosa* Susceptibility to Antibiotics and Reduces Its Pathogenesis in Host. *Curr*
765 *Microbiol* **77:** 479–490
766 Monaco H, Sereno T, Liu K, Reagor C, Deforet M & Xavier JB (2020) Spatial-temporal
767 dynamics of a microbial cooperative behavior robust to cheating. *BioRxiv*
768 Mulvey MR, Sorby PA, Triggs-Raine BL & Loewen PC (1988) Cloning and physical
769 characterization of *katE* and *katF* required for catalase HPII expression in *Escherichia*
770 *coli*. *Gene* **73:** 337–345
771 Nogales J, Gudmundsson S, Duque E, Ramos JL & Palsson BO (2017) Expanding The
772 Computable Reactome In *Pseudomonas putida* Reveals Metabolic Cycles Providing
773 Robustness. *BioRxiv*
774 Nogales J, Mueller J, Gudmundsson S, Canalejo FJ, Duque E, Monk J, Feist AM, Ramos JL,
775 Niu W & Palsson BO (2020) High-quality genome-scale metabolic modelling of
776 *Pseudomonas putida* highlights its broad metabolic capabilities. *Environ. Microbiol.*
777 **22:** 255–269
778 Overhage J, Lewenza S, Marr AK & Hancock REW (2007) Identification of genes involved
779 in swarming motility using a *Pseudomonas aeruginosa* PAO1 mini-Tn5-lux mutant
780 library. *J. Bacteriol.* **189:** 2164–2169
781 Paradis E & Schliep K (2019) ape 5.0: an environment for modern phylogenetics and
782 evolutionary analyses in R. *Bioinformatics* **35:** 526–528

783 Perry AC, Ni Bhriain N, Brown NL & Rouch DA (1991) Molecular characterization of the
784 *gor* gene encoding glutathione reductase from *Pseudomonas aeruginosa*:
785 determinants of substrate specificity among pyridine nucleotide-disulphide
786 oxidoreductases. *Mol. Microbiol.* **5:** 163–171
787 Pessi G & Haas D (2000) Transcriptional control of the hydrogen cyanide biosynthetic genes
788 *hcnABC* by the anaerobic regulator ANR and the quorum-sensing regulators LasR and
789 RhlR in *Pseudomonas aeruginosa*. *J. Bacteriol.* **182:** 6940–6949
790 Piatkov KI, Vu TTM, Hwang C-S & Varshavsky A (2015) Formyl-methionine as a
791 degradation signal at the N-termini of bacterial proteins. *Microb. Cell* **2:** 376–393
792 Picart-Armada S, Fernández-Albert F, Vinaixa M, Rodríguez MA, Aivio S, Stracker TH,
793 Yanes O & Perera-Lluna A (2017) Null diffusion-based enrichment for metabolomics
794 data. *PLoS One* **12:** e0189012
795 Picart-Armada S, Fernández-Albert F, Vinaixa M, Yanes O & Perera-Lluna A (2018)
796 FELLA: an R package to enrich metabolomics data. *BMC Bioinformatics* **19:** 538
797 Puertollano MA, Puertollano E, de Cienfuegos GÁ & de Pablo MA (2011) Dietary
798 antioxidants: immunity and host defense. *Curr. Top. Med. Chem.* **11:** 1752–1766
799 Py B & Barras F (2010) Building Fe-S proteins: bacterial strategies. *Nat. Rev. Microbiol.* **8:**
800 436–446
801 Redestig H, Fukushima A, Stenlund H, Moritz T, Arita M, Saito K & Kusano M (2009)
802 Compensation for systematic cross-contribution improves normalization of mass
803 spectrometry based metabolomics data. *Anal. Chem.* **81:** 7974–7980
804 Schmidt R, Ulanova D, Wick LY, Bode HB & Garbeva P (2019) Microbe-driven chemical
805 ecology: past, present and future. *ISME J.* **13:** 2656–2663
806 Smith E & Morowitz HJ (2004) Universality in intermediary metabolism. *Proc. Natl. Acad.*
807 *Sci. USA* **101:** 13168–13173

808 Stickland HG, Davenport PW, Lilley KS, Griffin JL & Welch M (2010) Mutation of *nfxB*
809 causes global changes in the physiology and metabolism of *Pseudomonas aeruginosa*.
810 *J. Proteome Res.* **9:** 2957–2967
811 Szenk M, Dill KA & de Graff AMR (2017) Why Do Fast-Growing Bacteria Enter Overflow
812 Metabolism? Testing the Membrane Real Estate Hypothesis. *Cell Syst.* **5:** 95–104
813 Thévenot EA, Roux A, Xu Y, Ezan E & Junot C (2015) Analysis of the Human Adult
814 Urinary Metabolome Variations with Age, Body Mass Index, and Gender by
815 Implementing a Comprehensive Workflow for Univariate and OPLS Statistical
816 Analyses. *J. Proteome Res.* **14:** 3322–3335
817 Tremblay J & Déziel E (2010) Gene expression in *Pseudomonas aeruginosa* swarming
818 motility. *BMC Genomics* **11:** 587
819 Vander Heiden MG, Cantley LC & Thompson CB (2009) Understanding the Warburg effect:
820 the metabolic requirements of cell proliferation. *Science* **324:** 1029–1033
821 de Vargas Roditi L, Boyle KE & Xavier JB (2013) Multilevel selection analysis of a
822 microbial social trait. *Mol. Syst. Biol.* **9:** 684
823 Vemuri GN, Altman E, Sangurdekar DP, Khodursky AB & Eiteman MA (2006) Overflow
824 metabolism in *Escherichia coli* during steady-state growth: transcriptional regulation
825 and effect of the redox ratio. *Appl. Environ. Microbiol.* **72:** 3653–3661
826 Vemuri GN, Eiteman MA, McEwen JE, Olsson L & Nielsen J (2007) Increasing NADH
827 oxidation reduces overflow metabolism in *Saccharomyces cerevisiae. Proc. Natl.*
828 *Acad. Sci. USA* **104:** 2402–2407
829 Vinckx T, Wei Q, Matthijs S & Cornelis P (2010) The *Pseudomonas aeruginosa* oxidative
830 stress regulator OxyR influences production of pyocyanin and rhamnolipids:
831 protective role of pyocyanin. *Microbiology (Reading, Engl.)* **156:** 678–686
832 Westbrock-Wadman S, Sherman DR, Hickey MJ, Coulter SN, Zhu YQ, Warrener P, Nguyen

833 LY, Shawar RM, Folger KR & Stover CK (1999) Characterization of a *Pseudomonas*
834 *aeruginosa* efflux pump contributing to aminoglycoside impermeability. *Antimicrob.*
835 *Agents Chemother.* **43:** 2975–2983
836 Xavier JB (2011) Social interaction in synthetic and natural microbial communities. *Mol.*
837 *Syst. Biol.* **7:** 483
838 Xavier JB, Kim W & Foster KR (2011) A molecular mechanism that stabilizes cooperative
839 secretions in *Pseudomonas aeruginosa*. *Mol. Microbiol.* **79:** 166–179
840 Xiao W & Loscalzo J (2019) Metabolic responses to reductive stress. *Antioxid. Redox Signal.*
841 Yan J, Deforet M, Boyle KE, Rahman R, Liang R, Okegbe C, Dietrich LEP, Qiu W & Xavier
842 JB (2017) Bow-tie signaling in c-di-GMP: Machine learning in a simple biochemical
843 network. *PLoS Comput. Biol.* **13:** e1005677
844 Yan J, Estanbouli H, Liao C, Kim W, Monk JM, Rahman R, Kamboj M, Palsson BO, Qiu W
845 & Xavier JB (2019) Systems-level analysis of NalD mutation, a recurrent driver of
846 rapid drug resistance in acute *Pseudomonas aeruginosa* infection. *PLoS Comput. Biol.*
847 **15:** e1007562
848 Yeung ATY, Bains M & Hancock REW (2011) The sensor kinase CbrA is a global regulator
849 that modulates metabolism, virulence, and antibiotic resistance in *Pseudomonas*
850 *aeruginosa. J. Bacteriol.* **193:** 918–931
851 Zhao B, Summers FA & Mason RP (2012) Photooxidation of Amplex Red to resorufin:
852 implications of exposing the Amplex Red assay to light. *Free Radic. Biol. Med.* **53:**
853 1080–1087
854 Zhu K, Chen S, Sysoeva TA & You L (2019) Universal antibiotic tolerance arising from
855 antibiotic-triggered accumulation of pyocyanin in *Pseudomonas aeruginosa. PLoS*
856 *Biol.* **17:** e3000573
857 Zhu K & Rock CO (2008) RhlA converts beta-hydroxyacyl-acyl carrier protein intermediates

in fatty acid synthesis to the beta-hydroxydecanoyl-beta-hydroxydecanoate component of rhamnolipids in *Pseudomonas aeruginosa. J. Bacteriol.* **190:** 3147–3154

863 **Table 1 Genes that are missing in non-rhamnolipid-producers but present in all**

864 **producers**

Non-producers	Missing genes
F5677	*arsB, arsC, arsH, arsR, chiC, dacB, fliM, gcd, qscR, gntK, gntR,*
F63912	*lasR*
H27930	*arnA, pelA, pcaB, pcaD, pfeA, icmF3, rrsmE, pcd, pirR, pctA,*
M1608	*tauD, opdG, pdxA, hcnC, hcnB, hcnA, glgA, ybhO, glgB, katE, glgP, ligD, ada, opdO, kynB, fusA2, cynR, cynT, cynS, cmrA, gor, galU, amrB, gnyD, gnyB, gnyH, gnyA, gnyL, hmgA, fahA, maiA,*
M55212	*crc, rph*
S86968	*kdsB, cysP, hcnC, hcnB, hcnA, pdxA, opdG, nfxB, cupB3*
W36662	*rhlR, rhlI, cupC1, pilC, pilS*
W60856	*lasR, pirA*

865

866 **Figures**

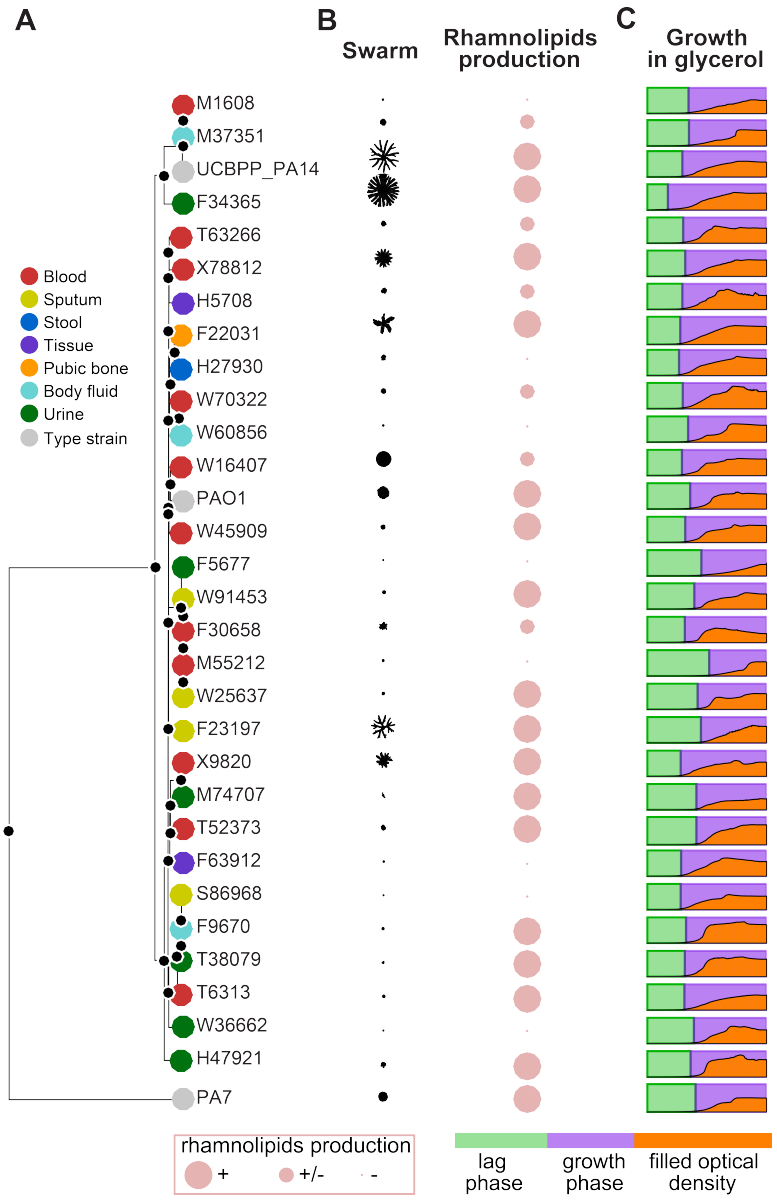

867

868 **Figure 1.** Diversity of swarming across the *P. aeruginosa* phylogeny of core genomes. **A.** Phylogeny
869 of clinical isolates obtained from patients with cancer at MSKCC (Yan *et al*, 2017, 2019) together
870 with reference type strains PAO1, PA14 and PA7. The tissue where each isolate was originally
871 isolated is labeled by circle colors. **B**. Swarming and rhamnolipid production phenotypes. The
872 swarming ability of these strains is represented by the actual swarming images on the agar plates (left
873 column). The ability of producing rhamnolipids of these strains is semi-quantitatively indicated by
874 circle sizes (right column). Both phenotypes do not correlate with phylogeny. All swarmers can

875 secrete rhamnolipids but some rhamnolipid producers cannot swarm. **C**. Growth curves in a synthetic
876 minimal medium using glycerol as the sole carbon source. Strain M6075 was excluded from
877 phylogenetic analysis due to the previous failure in sequencing and assembling its genome.

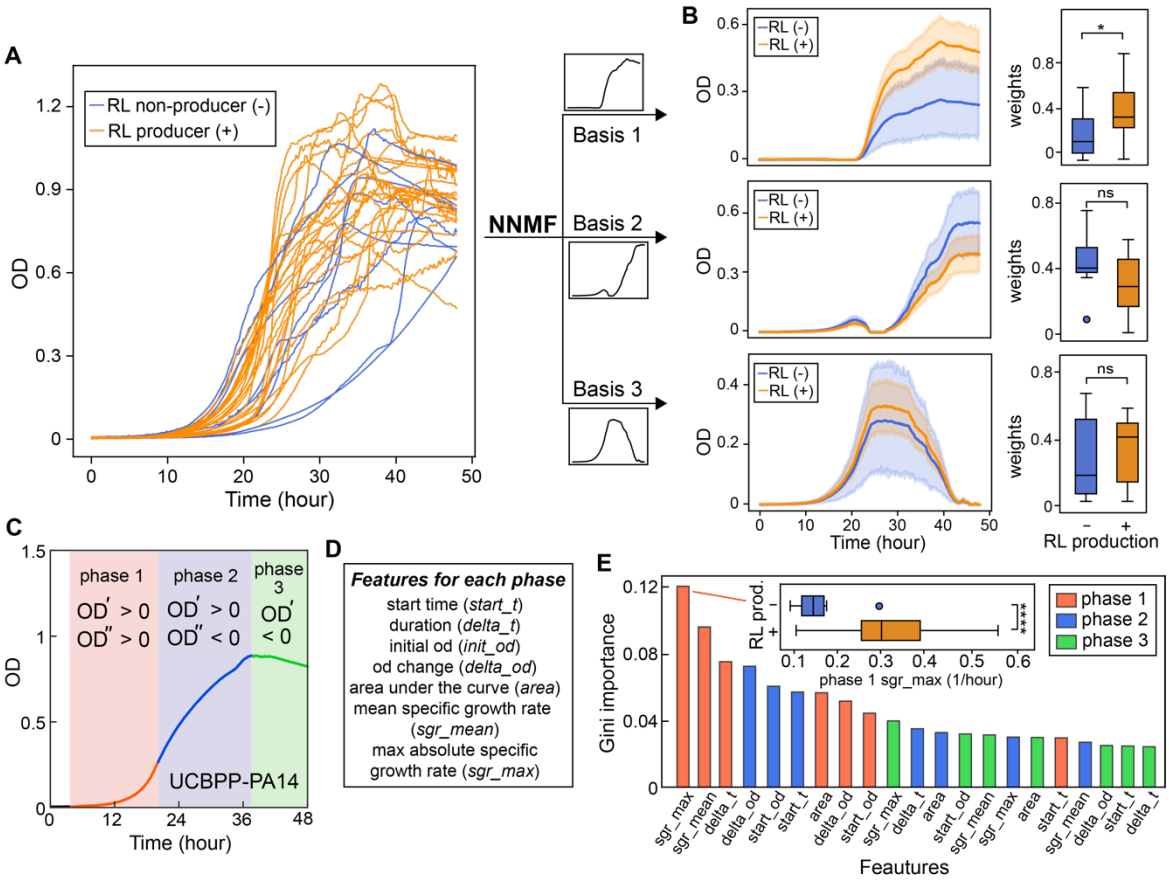

878

879 **Figure 2.** Growth curve features distinguish rhamnolipid producers from non-producers. **A,B.**
880 Unsupervised feature selection using non-negative matrix factorization (NNMF), which decomposes
881 growth curves of all *Pseudomonas* isolates into three additive basis functions (features) such that each
882 growth curve can be approximately represented by the weighted sum of these functions. **A**. Growth
883 curves from both rhamnolipid producers (orange) and non-producers (blue). **B**. Decomposed
884 components (basis function multiplied by weights; left panels) and weights (right panels) from NNMF
885 grouped by rhamnolipid (RL) production. The shaded areas represent 95% bootstrap confidence
886 interval of the mean. **C-E**. Supervised feature selection using Random Forest classifier. **C,D**. Feature
887 extraction method. Each growth curve (excluding the initial lag phase) was divided into three phases
888 (**C**) and each phase was described by 7 quantitative features (**D**). **E.** Ranking of feature importance in

classifying rhamnolipid producers. Inset: boxplot of maximum specific growth rate of phase I grouped by rhamnolipid production. Welch's t-test was used in (**B**) and (**E**) for significance testing. ****, p-value ≤ 0.0001; *, p-value ≤0.05; ns, p-value > 0.05.

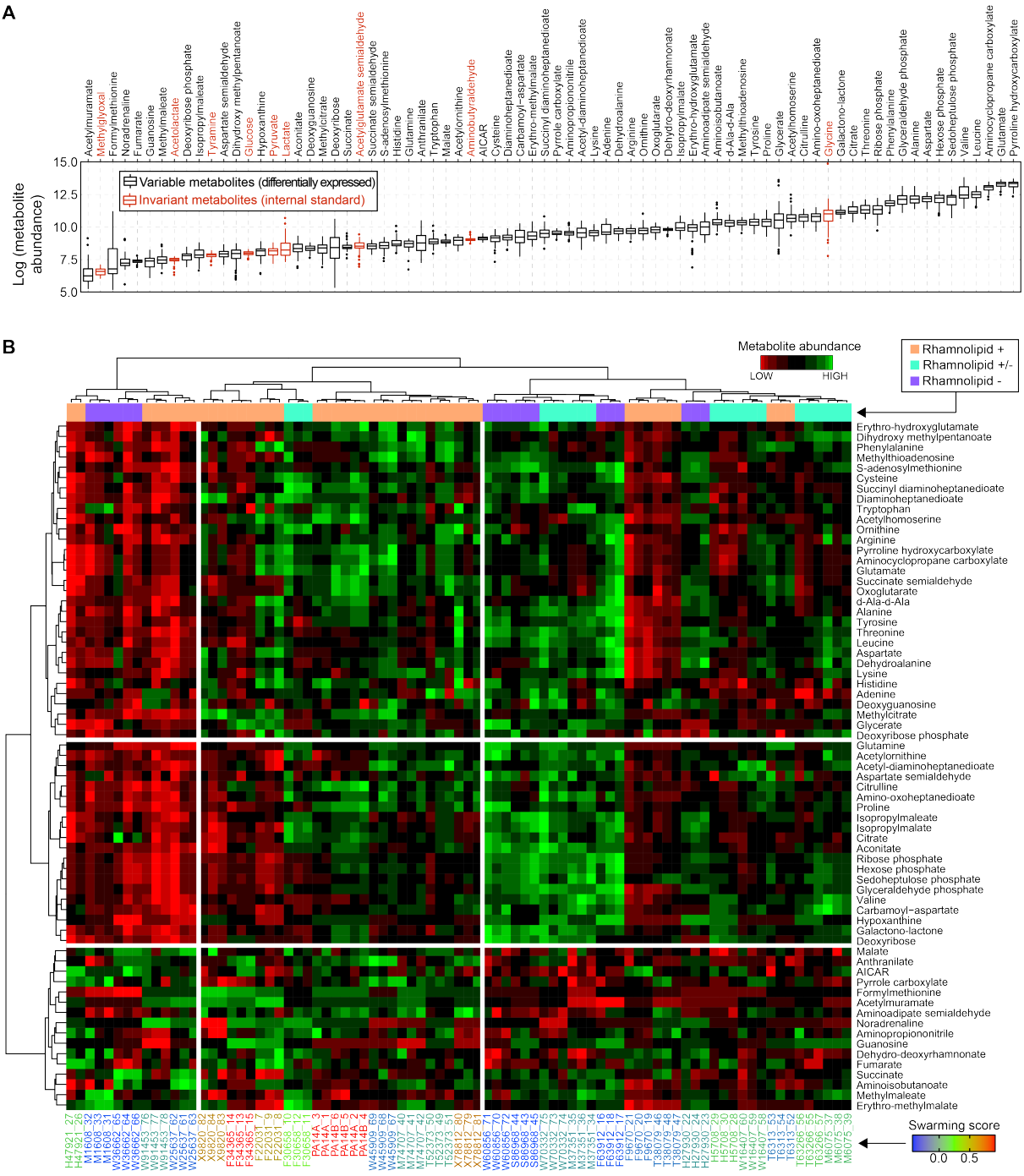

894 **Figure 3. Variance and clustering analysis of metabolomics across *Pseudomonas aeruginosa***
895 **strains. A.** Logarithm of raw peak area of all metabolites identified by LC-MS (Liquid
896 chromatography-Mass spectrometry). The metabolites in red were used as internal standard in the data
897 normalization step but removed from the dataset afterwards. **B.** Hierarchical clustering of the
898 metabolic profiles using Euclidean distance and Ward aggregation method. Each row represents one
899 metabolite and each column represents a specific sample (both strain and sample number are
900 indicated).

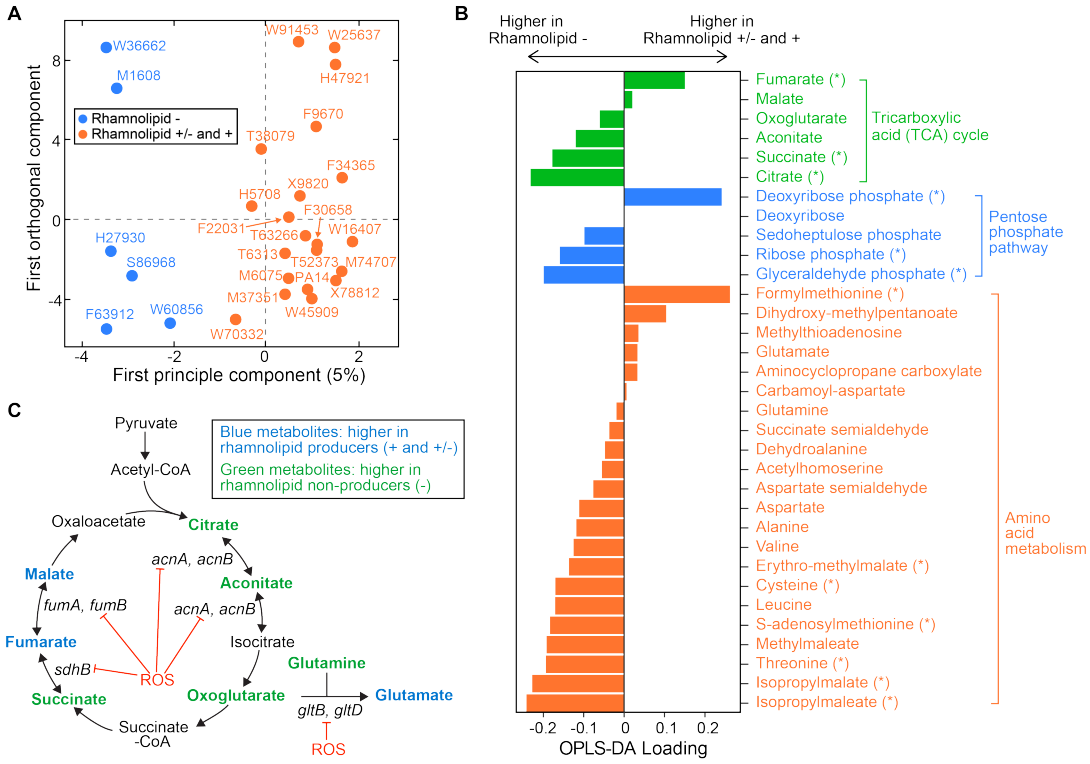

901

902 **Figure 4. Comparative metabolomics between rhamnolipid producers (include both mild and**
903 **strong production levels) and non-producers. A.** The scores plot of the OPLS-DA (orthogonal
904 partial least squares discriminant analysis) model. The first principle component separated the
905 rhamnolipid non-producers from producers. **B.** OPLS-DA loading values for the first principle
906 component of a selected number of metabolites. Metabolites with asterisk (*) are significantly
907 different between producers and non-producers (adjusted p-value of a Mann-Whitney test < 0.05). **C.**
908 Differential abundance of metabolites involved in reactions catalyzed by some Fe-S-containing
909 enzymes whose activities are inhibited by reactive oxygen species (ROS). Abbreviations: *acnA*

910 (aconitate hydratase A), *acnB* (aconitate hydratase B), *sdhB* (succinate dehydrogenase subunit), *fumA*
911 (fumarase A), *fumB* (fumarase B), *gltB* (glutamate synthase subunit), *gltD* (glutamate synthase
912 subunit).

913

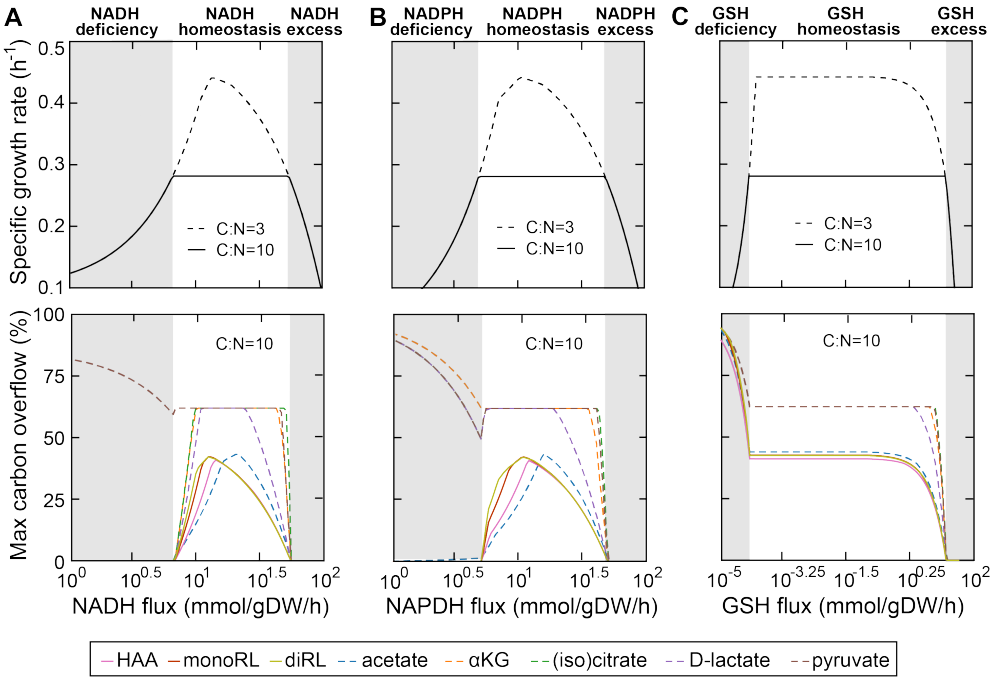

914

915 **Figure 5** Growth and rhamnolipid secretion are constrained by redox status. The redox stress levels
916 are perturbed by altering fluxes of NADH (**A.** reduced nicotinamide adenine dinucleotide) NADPH
917 (**B.** reduced nicotinamide adenine dinucleotide phosphate) and GSH (**C.** reduced glutathione). Upper
918 panels are predicted maximum growth rates and lower panels are predicted maximum byproduct
919 secretion fluxes. C:N indicates the carbon-to-nitrogen ratio between glycerol and ammonium in the
920 culture medium. C:N=3 and C:N=10 represent carbon- and nitrogen-limiting conditions respectively.
921 Abbreviations: HAA: 3-(3-hydroxyalkanoyloxy) alkanoate; monoRL: monorhamnolipid; diRL:
922 dirhamnolipid; aKG: alpha-ketoglutarate.

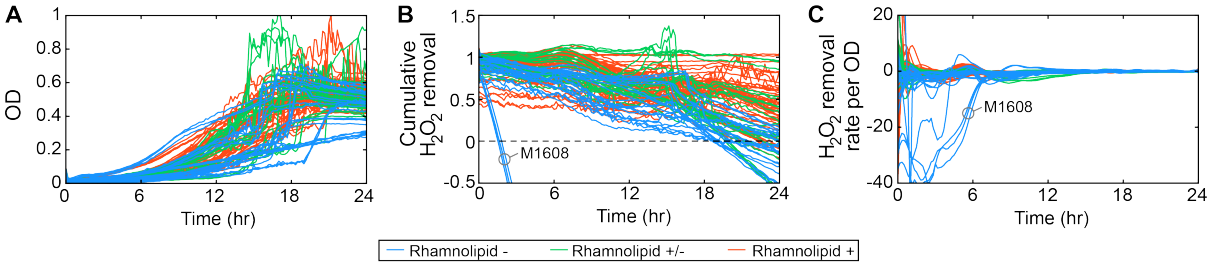

Figure 6. Comparison of the ability of removing culture medium hydrogen peroxide (H_2O_2) among strong rhamnolipid producers (+), weak producers (+/-), and non-producers (-). **A.** Population density. **B.** The total amount of hydrogen peroxide removed from the environment. Negative values indicate net cellular production of hydrogen peroxide released to the environment. **C.** The specific hydrogen peroxide removal rate. In both **B** and **C**, each trajectory of H_2O_2 fluorescence intensity was normalized to the averaged trajectory of the wild-type UCBPP-PA14 strain.

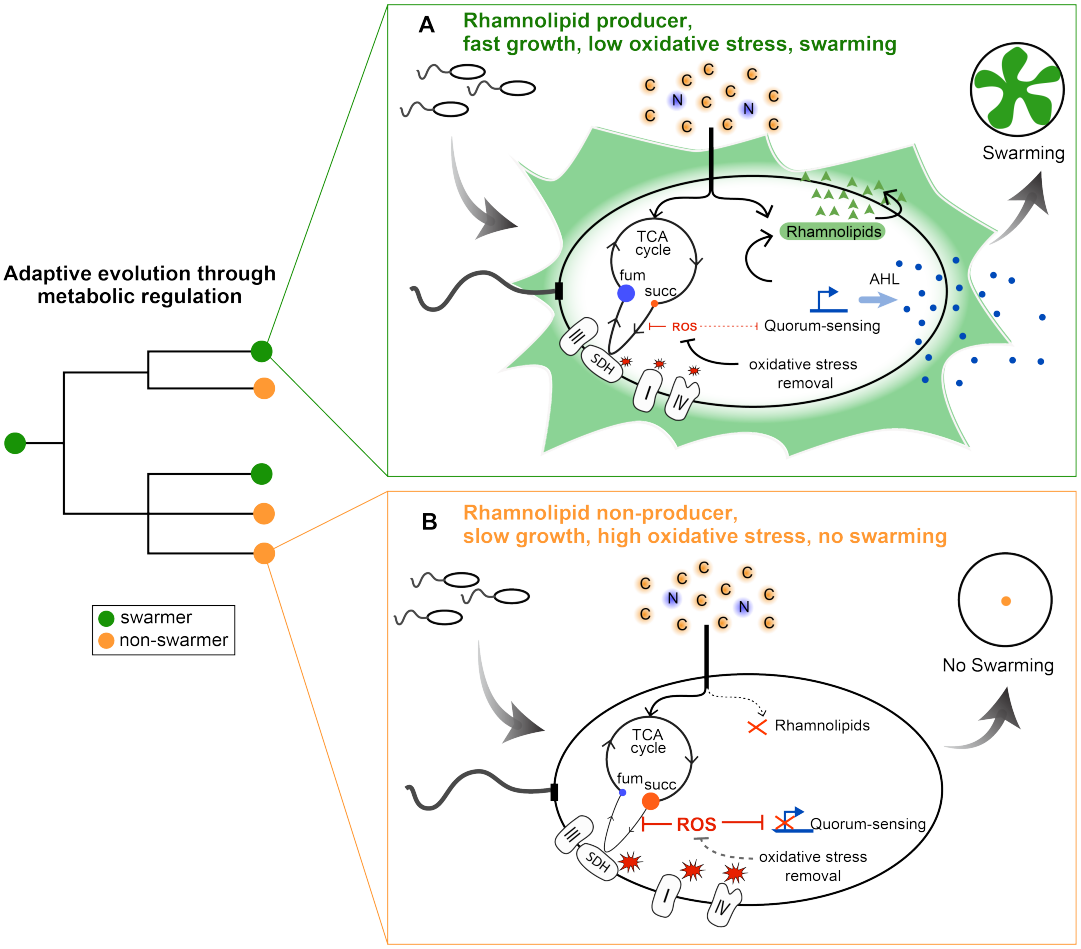

930

931

932 **Figure 7**. Schematic model showing how metabolism regulates evolution of swarming and
933 rhamnolipid production in *P. aeruginosa*. During aerobic growth, cells rely on the TCA cycle and
934 electron transport chain for central energy metabolism, which generates ROS (reactive oxygen
935 species) as byproduct. Particularly, the membrane-located succinate dehydrogenase (SDH), which
936 oxidizes succinate (succ in short, red dot, lower in rhamnolipid producers) to fumarate (fum in short,
937 blue dot, higher in rhamnolipid producers), is an important site of ROS production and serves as the
938 bottleneck of TCA cycle when ROS is excessive. **A.** Rhamnolipid producers are able to effectively
939 remove ROS; therefore, their TCA cycle fluxes are only minimally inhibited by ROS and remain high
940 to support fast growth. When cells reach certain density and nitrogen becomes limited, rhamnolipid
941 production is turned on by quorum-sensing. **B.** Rhamnolipid non-producers ineffectively remove ROS
942 and excessive ROS inhibits SDH, resulting in higher level of succinate and lower level of fumarate
943 compared to rhamnolipid producers. The ROS-mediated inhibition significantly slows down the TCA

944 cycle and cell growth. The increased ROS level is thought to impair quorum-sensing in non-producers
945 and subsequently abolishes rhamnolipid production under the same culture medium of producers. Our
946 model further suggests that null mutations and entire loss of genes that play important roles in redox
947 stress sensing, signaling and protection drive the observed diversity of swarming and rhamnolipid
948 production phenotypes along evolution.

949 **Supplementary Figures**

950

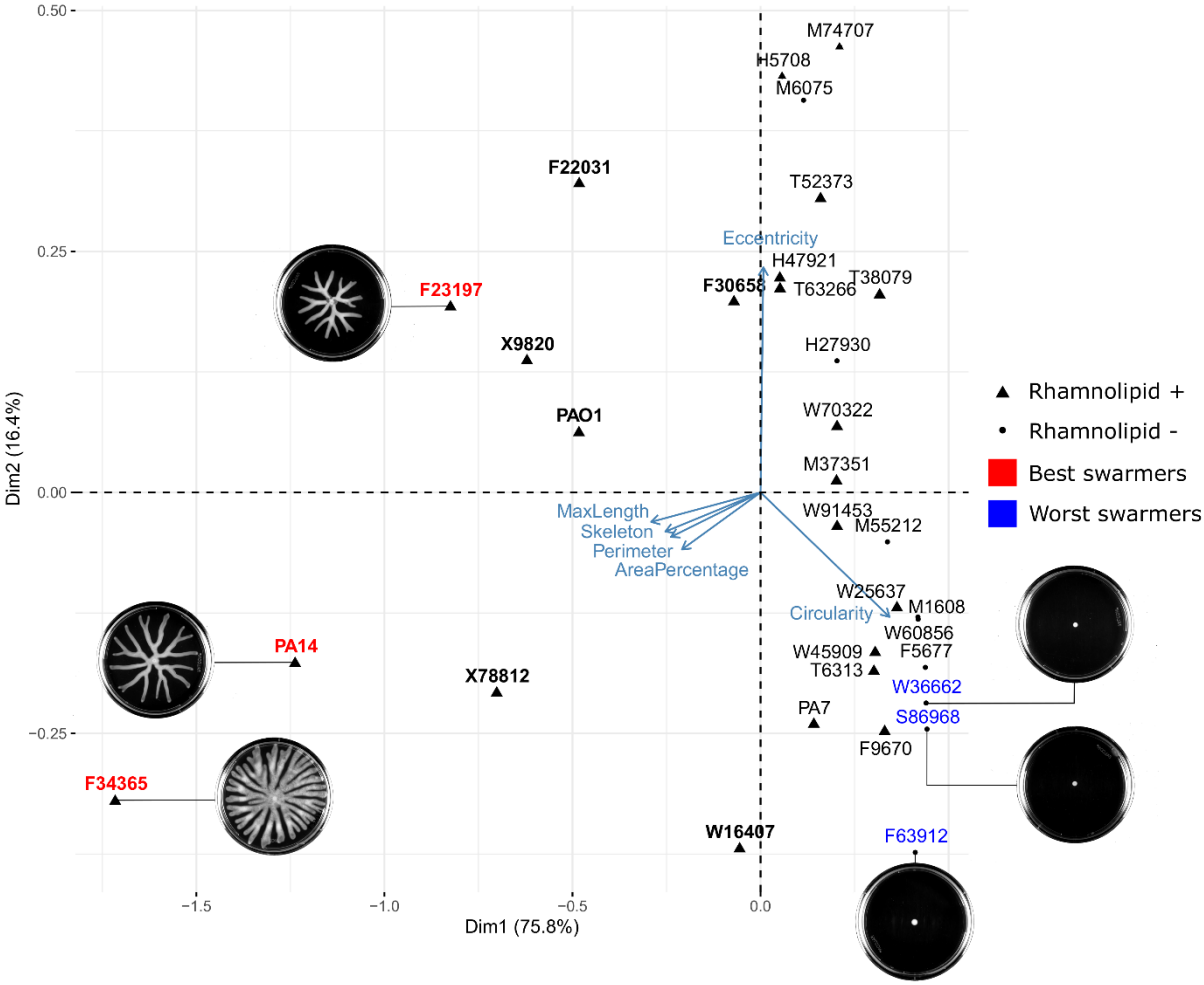

951

952 **Supplementary Figure 1.** Principle component analysis and biplot of the swarming phenotype. Six
953 morphological features were extracted from quantitative imaging analysis (see **Materials and**
954 **Methods** in the main text), including maximum length (MaxLength), skeleton, perimeter, area of
955 swarming colony (AreaPercentage), circularity and eccentricity. The MaxLength and circularity were
956 the top two features that separate strong swarmers (bold font-weight) from weak swarmers (normal
957 font-weight). The top 3 strains that have visually the largest (best swarmers) and smallest (worst
958 swarmers) swarming colonies are highlighted in red and blue respectively with their swarming images

959 shown alongside. The abilities of these strains to produce rhamnolipids are also indicated by triangles

960 (producers) and dots (non-producers).

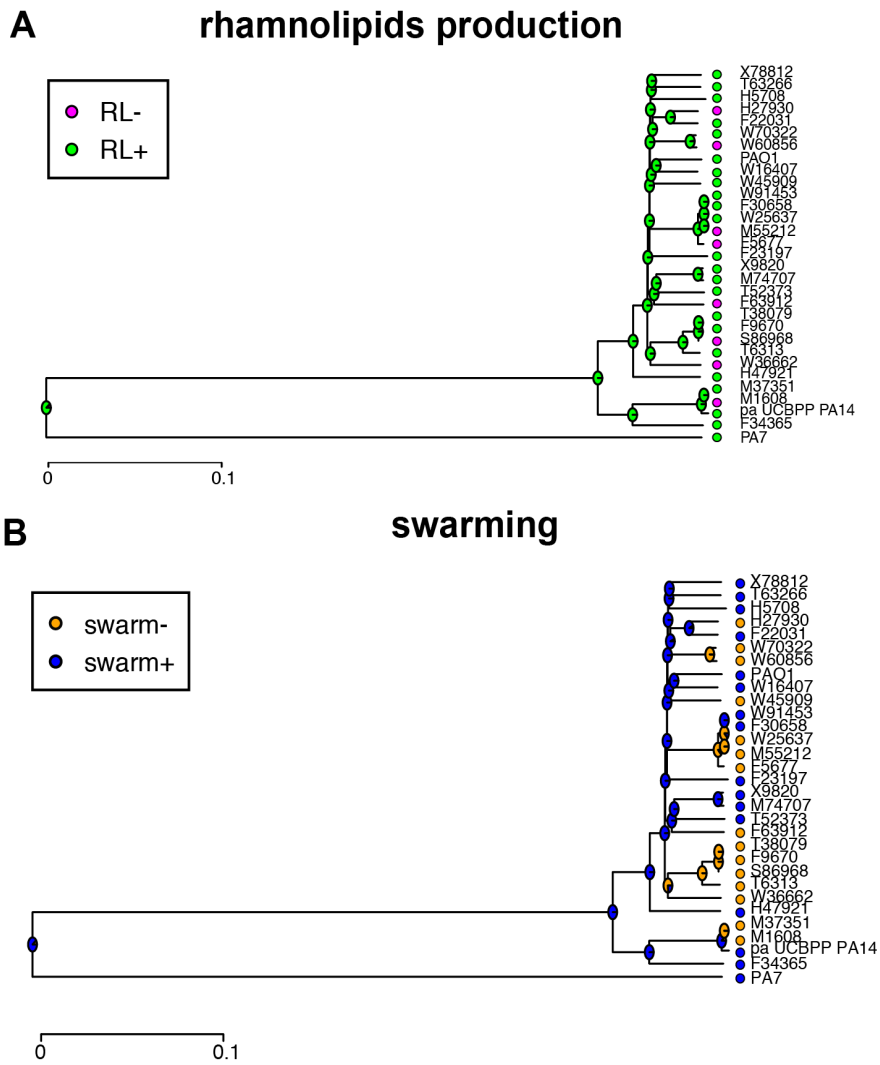

961

962 **Supplementary Figure 2.** Phylogenetic ancestor state reconstruction of rhamnolipid production (A)

963 and swarming phenotypes (B). For both (A) and (B), pie charts at the ancestor nodes of branches

964 represent relative likelihood proportion of each possible phenotypic state. We rooted the tree with

965 PA7, a *P. aeruginosa* isolate that is often used as an outlier to root phylogenetic trees. RL,

966 rhamnolipid production.

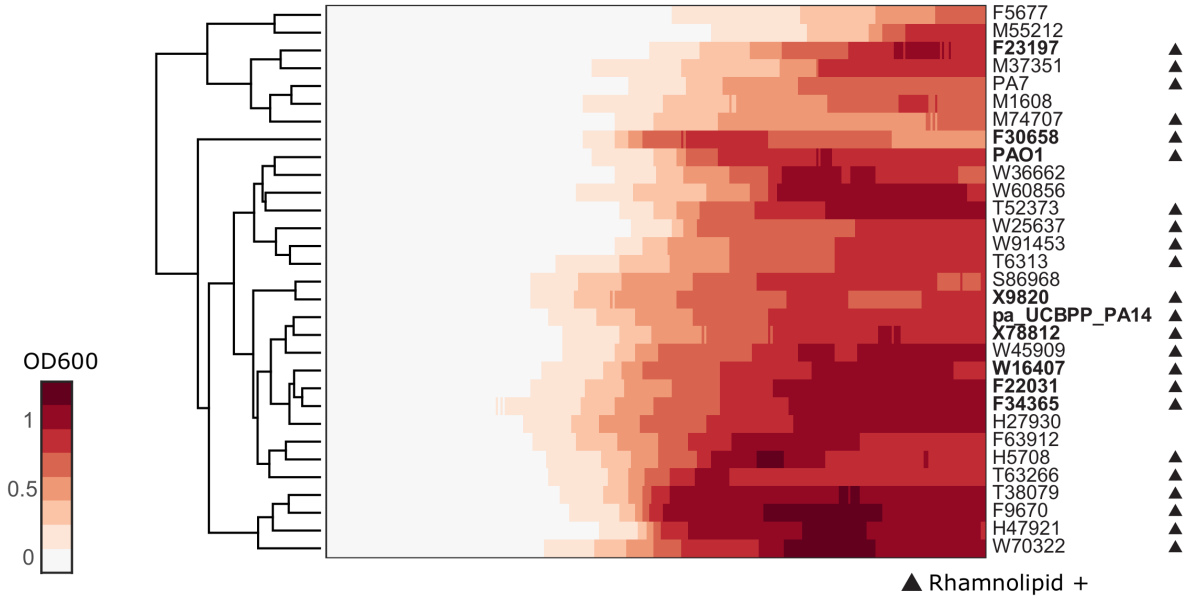

Supplementary Figure 3. Clustergram of growth curves of *P. aeruginosa* clinical isolates and three type strains PA14, PAO1 and PA7 in glycerol minimal medium. Euclidean distance was used as the measure of similarity. The strains that are able to swarm are indicated in bold. Most of the swarmers are clustered together. The swarmers that do not fall into this cluster include F30658 and PAO1, both of which are mild swarmers, as well as F23197 whose growth curve has a relatively longer lag time.

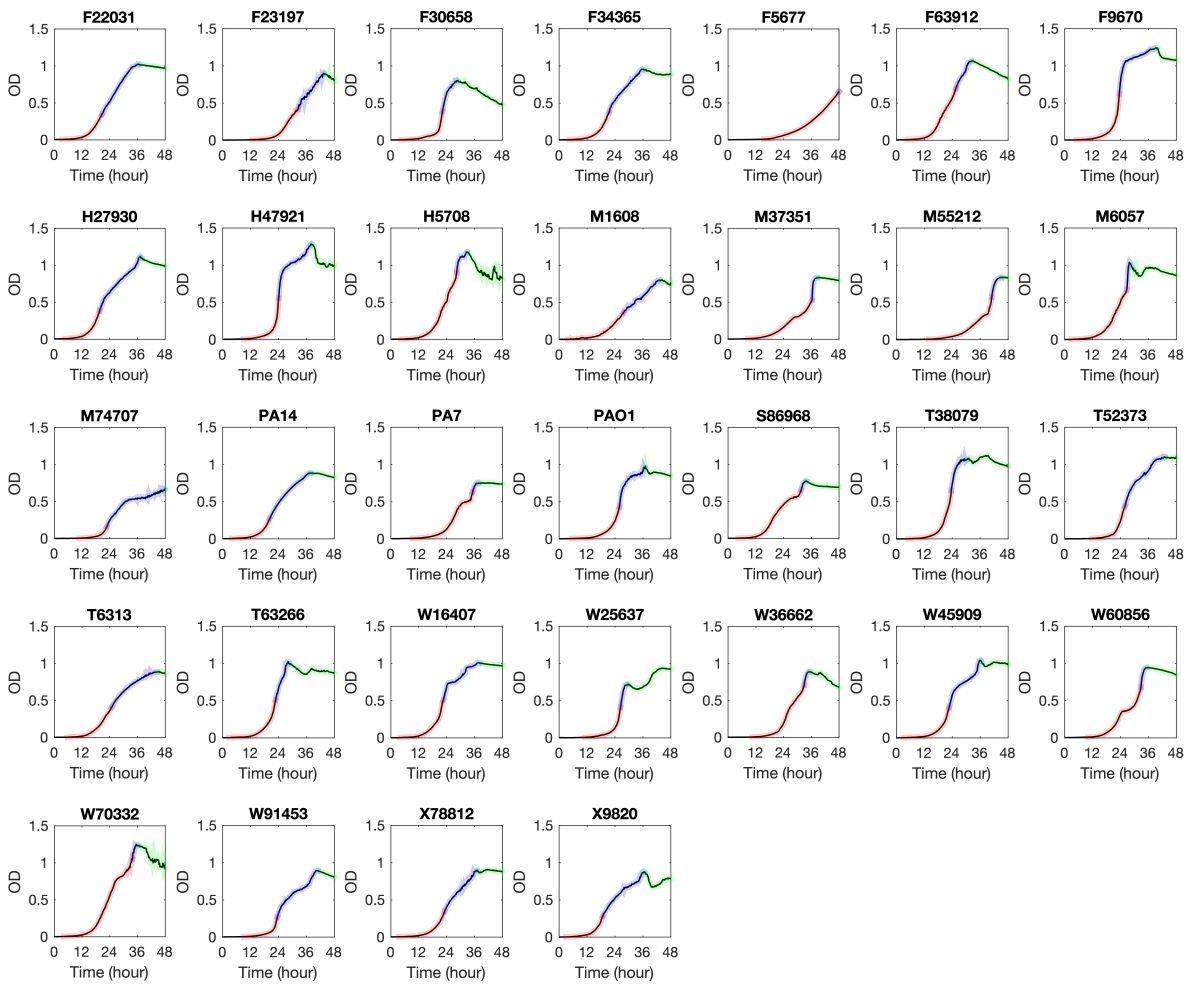

Supplementary Figure 4. Growth curve of *P. aeruginosa* strains in glycerol minimal medium. Phase I, II, and III are colored by red, blue and green respectively.

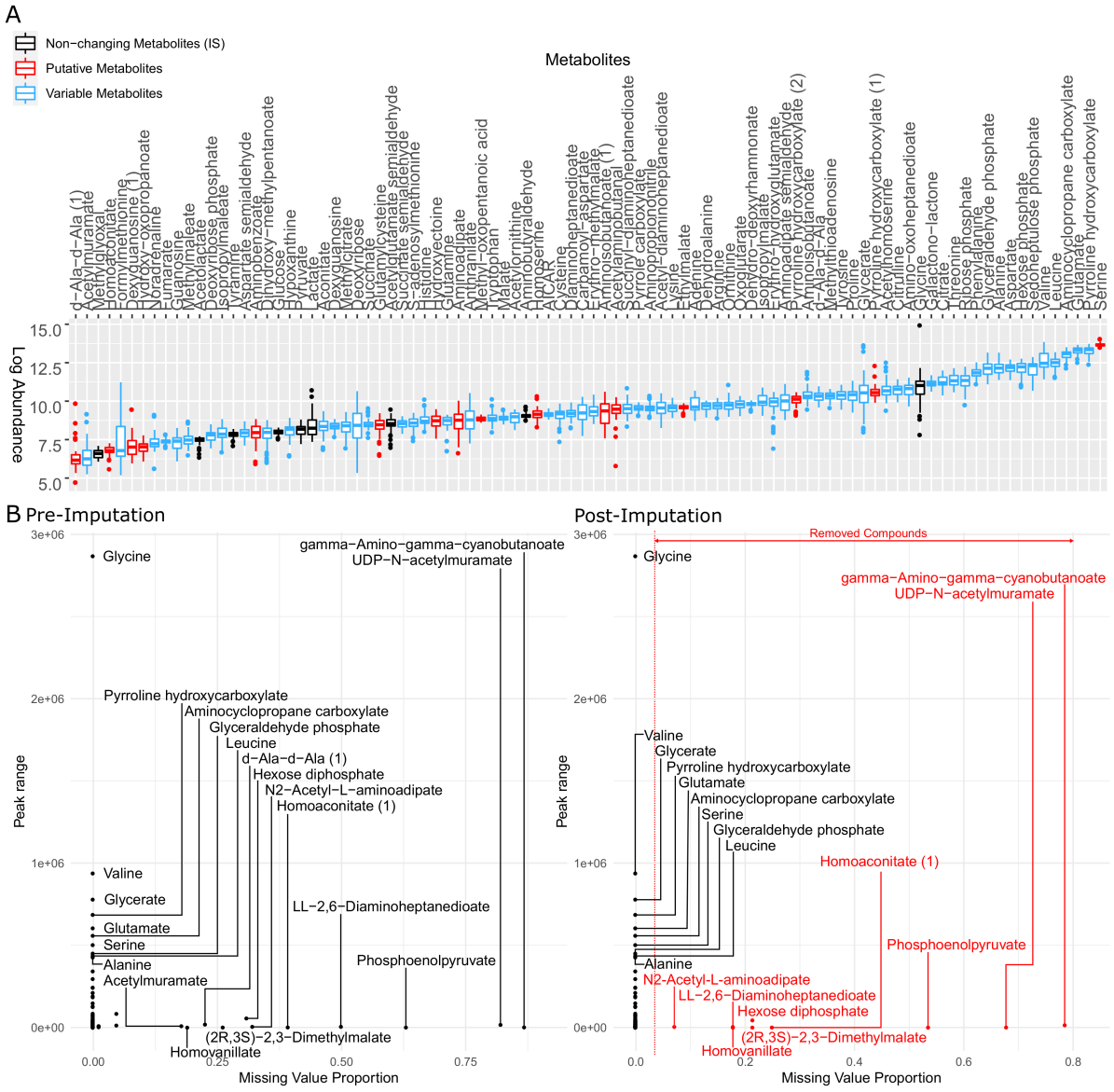

Supplementary Figure S5. A. The same as Fig. 3A of the main text but additionally includes metabolites with putative molecular identifications. These putative metabolites were initially included in clustering metabolomics but later removed from the heatmap (Fig. 3B of the main text). **B.** Metabolite peak area before (left panel) and after (right panel) imputation. The missing value proportion of a metabolite in the x-axis represents the frequency of missing values of the metabolite across all replicates of all strains in our study. The peak range of a metabolite in the y-axis is defined as the maximum peak area minus the minimum peak area among all non-missing values of the same metabolite across all our strains.

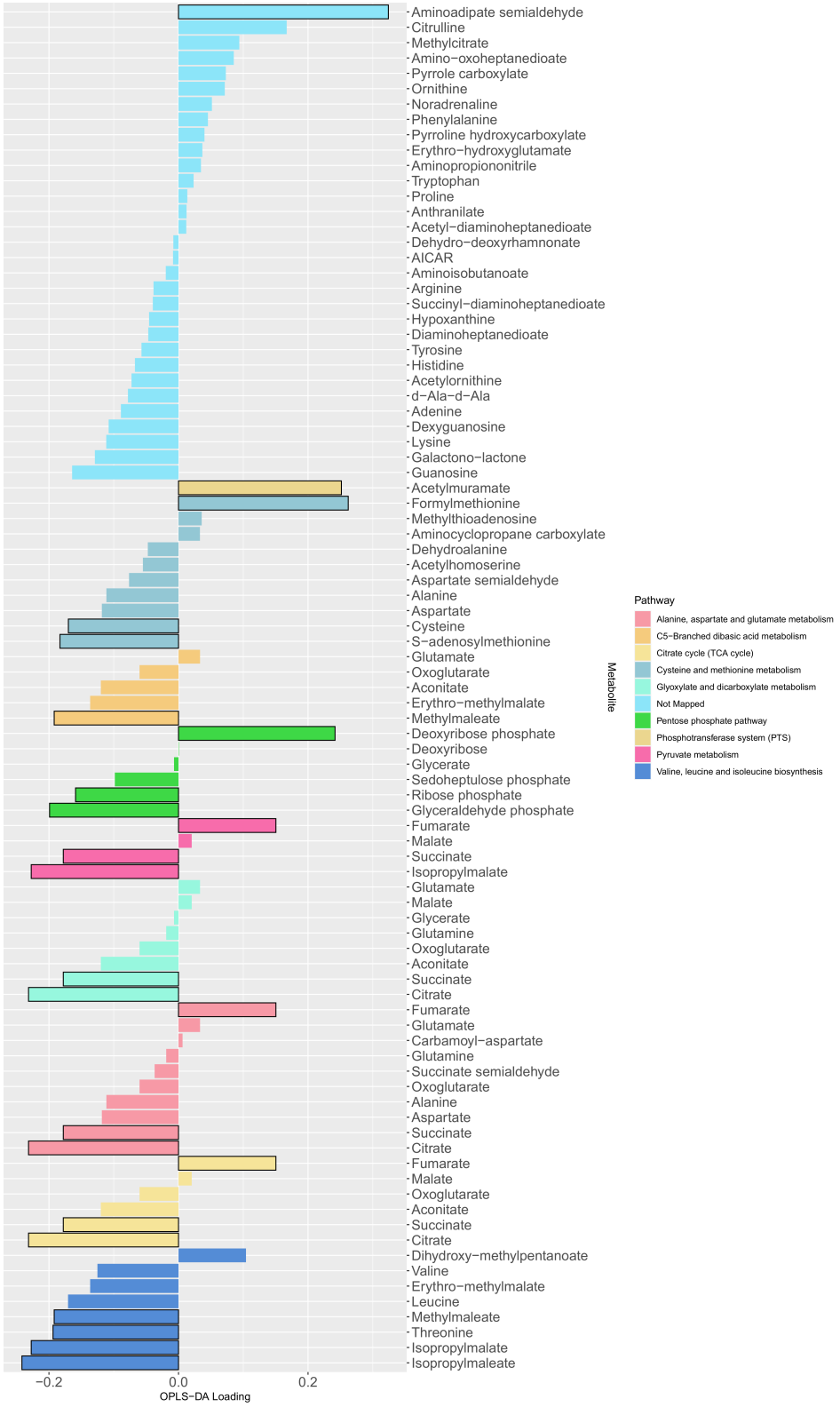

Supplementary Figure 6. The loading values of all predictive metabolites of the OPLS-DA model. The differential metabolites between producers and non-producers were determined by a Mann Whitney test (adjusted *p*-values with Benjamini-Hochberg method) with a level of significance of

991 0.05 (bars with black outline) and used as input for a metabolic pathway enrichment with FELLA
992 algorithm. The colors indicate the mapped metabolite pathway for each metabolite.

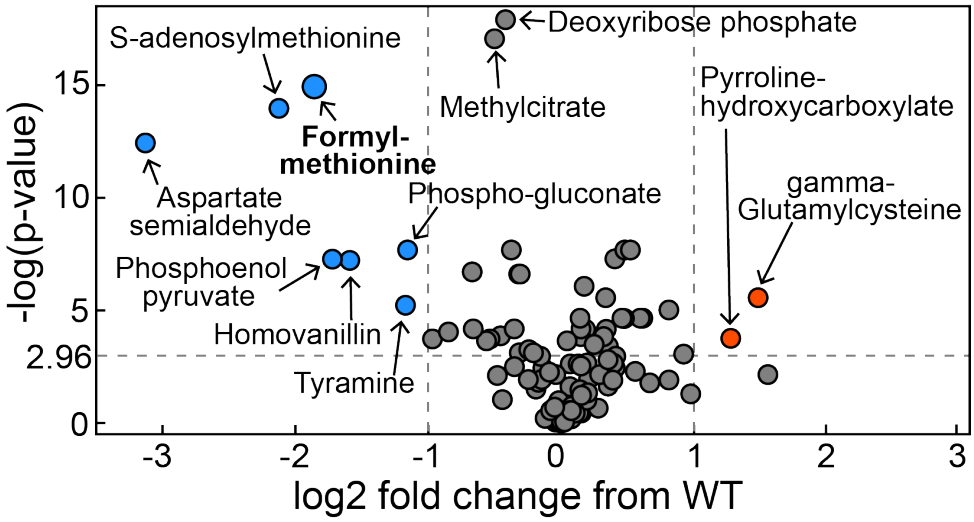

993

994 **Supplementary Figure 7.** Volcano plot of metabolomics data between wild-type *P. aeruginosa*
995 UCBPP-PA14 strain and its *rhlA* mutant grown in glycerol minimal medium (replotted with
996 permission from (Boyle *et al*, 2017)).

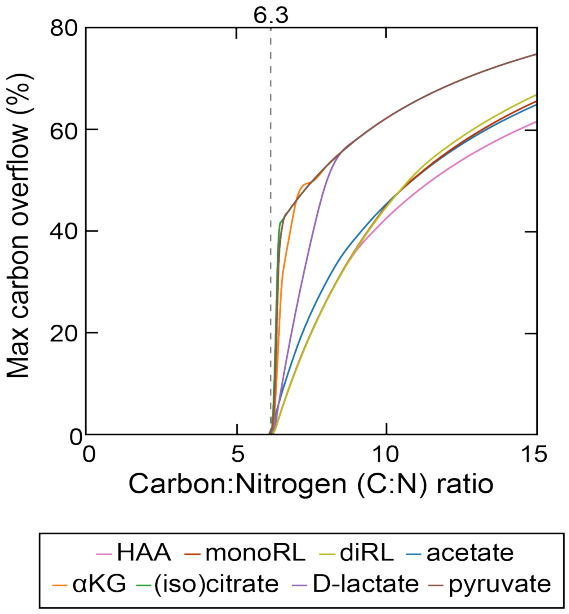

Supplementary Figure 8. Theoretical estimation of threshold carbon (glycerol):nitrogen (ammonium) ratio above which carbon is in excess in the sense that carbon release through rhamnolipids and central carbon metabolites does not compromise biomass production. Abbreviations: HAA: 3-(3-hydroxyalkanoyloxy)alkanoate; monoRL: monorhamnolipid; diRL: dirhamnolipid; aKG: alpha-ketoglutarate.

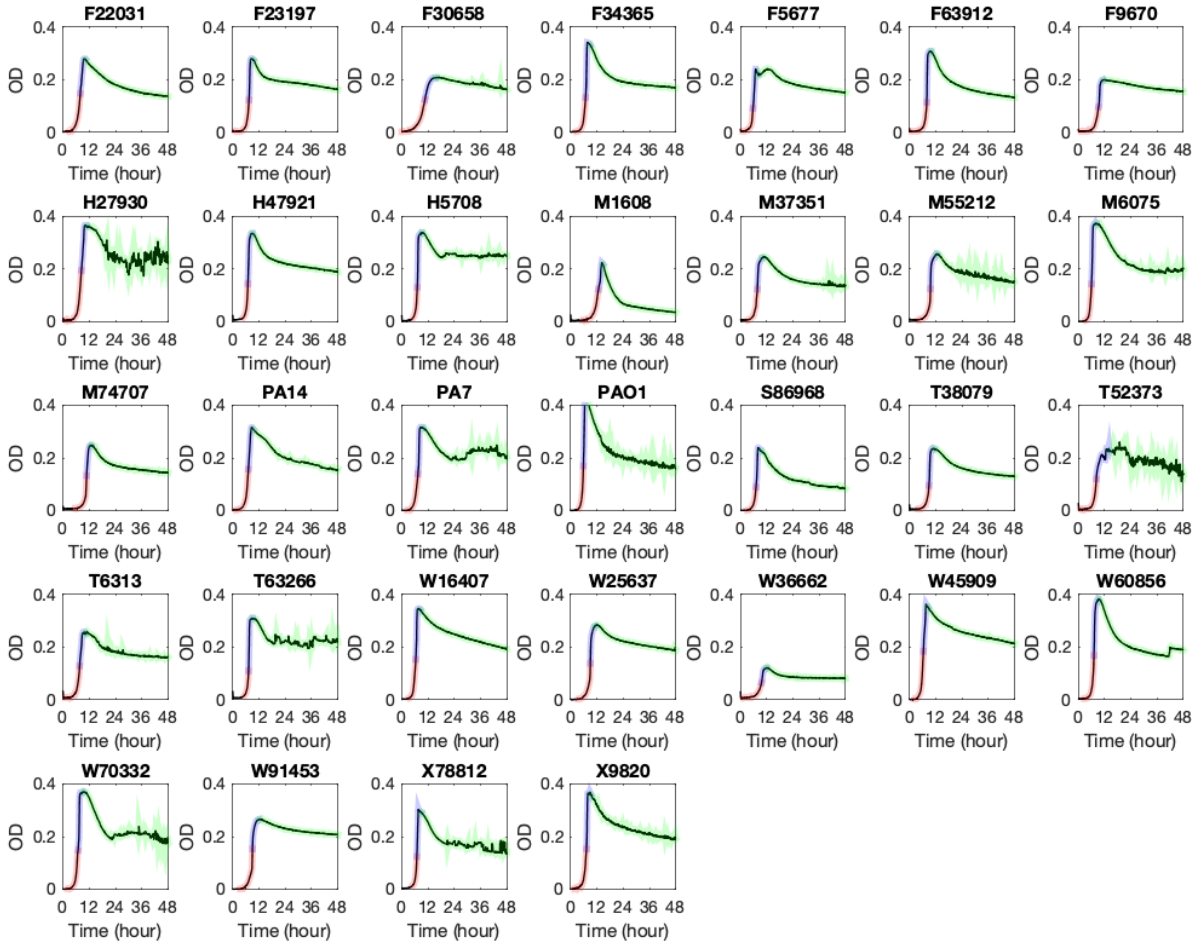

1004

1005 **Supplementary Figure 9.** Growth curve of *Pseudomonas aeruginosa* strains in succinate minimal

1006 medium. Phase I, II, and III are colored by red, blue and green respectively.

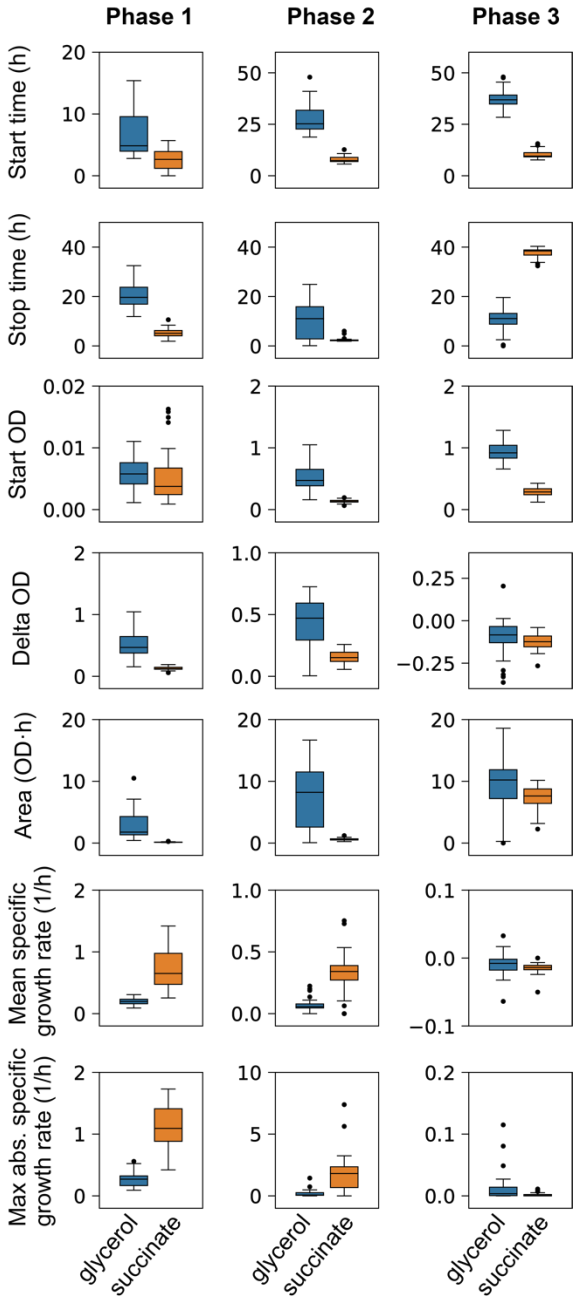

1007

1008 **Supplementary Figure 10.** Comparison of growth curve features of *Pseudomonas aeruginosa* strains

1009 grown in glycerol and succinate minimal medium.

1010 **Supplementary Data**

1011 **Supplementary Table 1:** output of the FELLA algorithm. A set of differential compounds was
1012 determined with a Mann-Whitney U test between rhamnolipid producers and rhamnolipid non
1013 producers (*p*-value adjusted with Benjamini-Hochberg method, alpha = 0.05). These compounds were
1014 used for applying diffusion algorithms over a graph consisting in all entries for *Pseudomonas*
1015 *aeruginosa* strain UCBPP-PA14 in KEGG database. The entries shown in the table are the ones with a
1016 significative probability of receiving part of the simulated flux.

KEGG.id	Entry.type	KEGG.name	p.score
pau00020	pathway	Citrate cycle (TCA cycle) - Pseudomonas aerug...	2.051E-02
pau00030	pathway	Pentose phosphate pathway - Pseudomonas aerug...	2.657E-04
pau00250	pathway	Alanine, aspartate and glutamate metabolism -...	3.502E-02
pau00270	pathway	Cysteine and methionine metabolism - Pseudomo...	3.106E-04
pau00290	pathway	Valine, leucine and isoleucine biosynthesis -...	1.000E-06
pau00620	pathway	Pyruvate metabolism - Pseudomonas aeruginosa ...	3.766E-02
pau00630	pathway	Glyoxylate and dicarboxylate metabolism - Pse...	1.105E-02
pau00660	pathway	C5-Branched dibasic acid metabolism - Pseudom...	8.242E-03
pau01503	pathway	Cationic antimicrobial peptide (CAMP) resista...	3.891E-02
pau02060	pathway	Phosphotransferase system (PTS) - Pseudomonas...	4.222E-02
M00001	module	Glycolysis (Embden-Meyerhof pathway), glucose...	1.613E-02
M00002	module	Glycolysis, core module involving three-carbo...	4.022E-03
M00003	module	Gluconeogenesis, oxaloacetate => fructose-6P	2.299E-03
M00004	module	Pentose phosphate pathway (Pentose phosphate ...	3.993E-03

M00005	module	PRPP biosynthesis, ribose 5P => PRPP	1.000E-06
M00007	module	Pentose phosphate pathway, non-oxidative phas...	1.030E-04
M00009	module	Citrate cycle (TCA cycle, Krebs cycle)	7.517E-04
M00010	module	Citrate cycle, first carbon oxidation, oxaloa...	4.789E-04
M00011	module	Citrate cycle, second carbon oxidation, 2-oxo...	8.189E-03
M00012	module	Glyoxylate cycle	1.577E-03
M00019	module	Valine/isoleucine biosynthesis, pyruvate => v...	5.143E-03
M00032	module	Lysine degradation, lysine => saccharopine =>...	2.928E-04
M00049	module	Adenine ribonucleotide biosynthesis, IMP => A...	3.245E-02
M00149	module	Succinate dehydrogenase, prokaryotes	4.051E-02
M00165	module	Reductive pentose phosphate cycle (Calvin cyc...	8.362E-04
M00167	module	Reductive pentose phosphate cycle, glyceralde...	2.917E-04
M00173	module	Reductive citrate cycle (Arnon-Buchanan cycle...	1.377E+09
M00308	module	Semi-phosphorylative Entner-Doudoroff pathway...	2.511E-02
M00344	module	Formaldehyde assimilation, xylulose monophosp...	5.467E-03
M00374	module	Dicarboxylate-hydroxybutyrate cycle	2.552E-02
M00432	module	Leucine biosynthesis, 2-oxoisovalerate => 2-o...	1.000E-06
M00535	module	Isoleucine biosynthesis, pyruvate => 2-oxobut...	1.000E-06
M00570	module	Isoleucine biosynthesis, threonine => 2-oxobu...	8.290E-04
M00620	module	Incomplete reductive citrate cycle, acetyl-Co...	1.000E-06
M00633	module	Semi-phosphorylative Entner-Doudoroff pathway...	3.830E-02
M00740	module	Methylaspartate cycle	4.398E-02
1.1.1.85	enzyme	3-isopropylmalate dehydrogenase	1.000E-06
1.2.1.12	enzyme	glyceraldehyde-3-phosphate dehydrogenase (pho...	1.578E-03

1.2.1.9	enzyme	glyceraldehyde-3-phosphate dehydrogenase (NAD...	4.815E-04
1.3.5.1	enzyme	succinate dehydrogenase	5.028E+08
1.3.5.4	enzyme	fumarate reductase (quinol)	5.028E+08
1.4.1.9	enzyme	leucine dehydrogenase	1.032E-02
1.8.4.15	enzyme	protein dithiol oxidoreductase (disulfide-for...	3.891E-02
2.2.1.1	enzyme	transketolase	1.838E+08
2.2.1.2	enzyme	transaldolase	5.939E-04
2.3.3.1	enzyme	citrate (Si)-synthase	1.000E-06
2.3.3.13	enzyme	2-isopropylmalate synthase	1.000E-06
2.4.2.1	enzyme	purine-nucleoside phosphorylase	1.000E-06
2.4.2.2	enzyme	pyrimidine-nucleoside phosphorylase	1.000E-06
2.5.1.49	enzyme	O-acetylhomoserine aminocarboxypropyltransfer...	4.137E-02
2.6.1.2	enzyme	alanine transaminase	1.000E-06
2.6.1.42	enzyme	branched-chain-amino-acid transaminase	1.985E-02
2.6.1.66	enzyme	valine---pyruvate transaminase	1.000E-06
2.7.1.15	enzyme	ribokinase	1.791E-02
2.7.1.221	enzyme	N-acetylmuramate 1-kinase	1.000E-06
2.7.2.3	enzyme	phosphoglycerate kinase	1.747E-02
2.7.6.1	enzyme	ribose-phosphate diphosphokinase	1.000E-06
2.7.9.2	enzyme	pyruvate, water dikinase	7.185E-03
2.8.3.18	enzyme	succinyl-CoA:acetate CoA-transferase	1.672E-02
3.1.3.105	enzyme	N-acetyl-D-muramate 6-phosphate phosphatase	1.000E-06
3.1.3.11	enzyme	fructose-bisphosphatase	3.302E-02
3.1.3.48	enzyme	protein-tyrosine-phosphatase	1.524E-02

3.2.2.10	enzyme	pyrimidine-5'-nucleotide nucleosidase	1.000E-06
3.2.2.4	enzyme	AMP nucleosidase	1.000E-06
3.4.21.107	enzyme	peptidase Do	1.929E-02
3.4.24.40	enzyme	serralysin	3.891E-02
3.5.1.28	enzyme	N-acetylmuramoyl-L-alanine amidase	1.000E-06
3.5.4.2	enzyme	adenine deaminase	1.786E-02
3.6.1.13	enzyme	ADP-ribose diphosphatase	7.396E+08
3.7.1.20	enzyme	3-fumarylpyruvate hydrolase	2.495E-02
4.1.1.31	enzyme	phosphoenolpyruvate carboxylase	4.009E-02
4.1.2.13	enzyme	fructose-bisphosphate aldolase	2.966E-03
4.1.2.14	enzyme	2-dehydro-3-deoxy-phosphogluconate aldolase	2.363E-02
4.1.2.48	enzyme	low-specificity L-threonine aldolase	9.416E-04
4.1.3.1	enzyme	isocitrate lyase	1.814E-02
4.2.1.2	enzyme	fumarate hydratase	1.000E-06
4.2.1.20	enzyme	tryptophan synthase	3.153E-02
4.2.1.3	enzyme	aconitate hydratase	1.000E-06
4.2.1.33	enzyme	3-isopropylmalate dehydratase	1.000E-06
4.2.1.35	enzyme	(R)-2-methylmalate dehydratase	1.000E-06
4.2.3.1	enzyme	threonine synthase	3.155E-02
4.3.1.1	enzyme	aspartate ammonia-lyase	1.000E-06
4.3.1.19	enzyme	threonine ammonia-lyase	1.000E-06
4.3.2.1	enzyme	argininosuccinate lyase	1.647E-02
4.3.2.2	enzyme	adenylosuccinate lyase	9.353E-04
5.1.3.1	enzyme	ribulose-phosphate 3-epimerase	1.624E-02
5.2.1.8	enzyme	peptidylprolyl isomerase	3.891E-02

5.3.1.1	enzyme	triose-phosphate isomerase	1.698E+08
5.3.1.6	enzyme	ribose-5-phosphate isomerase	2.338E-02
5.4.2.2	enzyme	phosphoglucomutase (alpha-D-glucose-1,6-bisph...	4.898E+09
6.2.1.5	enzyme	succinate---CoA ligase (ADP-forming)	6.932E-03
6.3.1.2	enzyme	glutamine synthetase	3.639E-02
6.4.1.1	enzyme	pyruvate carboxylase	4.182E+07
R00086	reaction	ATP phosphohydrolase	3.936E-02
R00122	reaction	ADP phosphohydrolase	3.029E-02
R00177	reaction	ATP:L-methionine S-adenosyltransferase	1.894E-02
R00182	reaction	AMP phosphoribohydrolase	1.000E-06
R00220	reaction	L-serine ammonia-lyase	2.595E-02
R00258	reaction	L-Alanine:2-oxoglutarate aminotransferase	4.726E-02
R00351	reaction	acetyl-CoA:oxaloacetate C-acetyltransferase (...	1.000E-06
R00352	reaction	acetyl-CoA:oxaloacetate C-acetyltransferase [...	1.000E-06
R00402	reaction	succinate:NAD+ oxidoreductase	1.000E-06
R00405	reaction	Succinate:CoA ligase (ADP-forming)	4.397E+09
R00432	reaction	Succinate:CoA ligase (GDP-forming)	2.166E-02
R00446	reaction	L-lysine:NAD+ 6-oxidoreductase (deaminating)	1.000E-06
R00479	reaction	isocitrate glyoxylate-lyase (succinate-formin...	3.522E-02
R00490	reaction	L-aspartate ammonia-lyase (fumarate-forming)	1.000E-06
R00510	reaction	cytidine-5'-monophosphate phosphoribohydrolas...	1.000E-06
R00653	reaction	N-formyl-L-methionine amidohydrolase	1.000E-06
R00751	reaction	L-threonine acetaldehyde-lyase (glycine-formi...	1.000E-06
R00782	reaction	L-cysteine hydrogen-sulfide-lyase (deaminatin...	1.000E-06
R00891	reaction	L-serine hydro-lyase (adding hydrogen sulfide...	1.000E-06

R00892	reaction	L-cysteine:NAD+ oxidoreductase	1.384E-02
R00893	reaction	L-Cysteine:oxygen oxidoreductase	7.899E-03
R00894	reaction	L-glutamate:L-cysteine gamma-ligase (ADP-form...	3.659E-03
R00895	reaction	L-Cysteine:2-oxoglutarate aminotransferase	1.786E-02
R00897	reaction	O3-acetyl-L-serine:hydrogen-sulfide 2-amino-2...	4.683E-03
R00901	reaction	L-cysteine hydrogen-sulfide-lyase (adding sul...	4.539E-03
R00994	reaction	(2R,3S)-3-methylmalate:NAD+ oxidoreductase	1.000E-06
R00996	reaction	L-threonine ammonia-lyase (2-oxobutanoate-for...	1.000E-06
R00999	reaction	O-Succinyl-L-homoserine succinate-lyase (deam...	2.925E-02
R01001	reaction	L-cystathionine cysteine-lyase (deaminating	3.769E-04
R01015	reaction	D-glyceraldehyde-3-phosphate aldose-ketose-is...	1.000E-06
R01049	reaction	ATP:D-ribose-5-phosphate diphosphotransferase	1.000E-06
R01051	reaction	ATP:D-ribose 5-phosphotransferase	1.000E-06
R01053	reaction	Ribose-5-phosphate:ammonia ligase (ADP-formin...	1.804E+07
R01054	reaction	ADP-ribose ribophosphohydrolase	9.884E+08
R01055	reaction	uracil hydro-lyase (adding D-ribose 5-phospha...	2.245E-03
R01056	reaction	D-ribose-5-phosphate aldose-ketose-isomerase	1.000E-06
R01057	reaction	D-Ribose 1,5-phosphomutase	1.000E-06
R01058	reaction	D-glyceraldehyde 3-phosphate:NADP+ oxidoreduc...	1.000E-06
R01059	reaction	ATP:D-glyceraldehyde 3-phosphotransferase	1.000E-06
R01061	reaction	D-glyceraldehyde-3-phosphate:NAD+ oxidoreduct...	1.357E-04
R01063	reaction	D-glyceraldehyde-3-phosphate:NADP+ oxidoreduc...	1.690E-04

R01066	reaction	2-deoxy-D-ribose-5-phosphate acetaldehyde-lya...	1.494E-04
R01067	reaction	D-Fructose 6-phosphate:D-glyceraldehyde-3-pho...	5.048E+08
R01068	reaction	D-fructose-1,6-bisphosphate D-glyceraldehyde-...	8.170E+09
R01069	reaction	D-tagatose 1,6-bisphosphate D-glyceraldehyde-...	4.029E-04
R01070	reaction	beta-D-fructose-1,6-bisphosphate D-glyceralde...	8.852E+08
R01082	reaction	(S)-malate hydro-lyase (fumarate-forming)	1.000E-06
R01083	reaction	N6-(1,2-dicarboxyethyl)AMP AMP-lyase (fumarat...	2.469E-03
R01085	reaction	3-fumarylpyruvate fumarylhydrolase	1.563E-02
R01086	reaction	2-(Nomega-L-arginino)succinate arginine-lyase...	5.126E-03
R01087	reaction	Maleate cis-trans-isomerase	2.433E+09
R01113	reaction	Glutathione:L-cystine oxidoreductase	3.593E-02
R01128	reaction	5'-Inosinate phosphoribohydrolase	1.000E-06
R01213	reaction	acetyl-CoA:3-methyl-2-oxobutanoate C-acetyltr...	1.000E-06
R01215	reaction	L-Valine:pyruvate aminotransferase	3.535E-02
R01244	reaction	Adenine aminohydrolase	2.846E-02
R01270	reaction	Nicotinamide D-ribonucleotide phosphoribohydr...	1.000E-06
R01322	reaction	Citrate:CoA ligase (ADP-forming)	3.624E-04
R01324	reaction	citrate hydroxymutase	1.000E-06
R01325	reaction	citrate hydro-lyase (cis-aconitate-forming)	1.000E-06
R01364	reaction	4-fumarylacetoacetate fumarylhydrolase	2.477E-02
R01440	reaction	D-Xylulose-5-phosphate:formaldehyde glycolald...	4.322E+09
R01465	reaction	L-threonine:NAD+ oxidoreductase	1.000E-06
R01466	reaction	O-phospho-L-homoserine phosphate-lyase (addin...	6.537E+09
R01561	reaction	adenosine:phosphate alpha-D-ribosyltransferas...	2.961E-03
R01570	reaction	thymidine:phosphate deoxy-alpha-D-ribosyltran...	1.000E-06

R01621	reaction	D-xylulose 5-phosphate D-glyceraldehyde-3-pho...	1.000E-06
R01641	reaction	sedoheptulose-7-phosphate:D-glyceraldehyde-3-...	1.000E-06
R01652	reaction	4-Methyl-2-oxopentanoate + CO2 <=> (2S)-2-Iso...	4.391E-03
R01827	reaction	sedoheptulose-7-phosphate:D-glyceraldehyde-3-...	1.594E-04
R01830	reaction	beta-D-Fructose 6-phosphate:D-glyceraldehyde-...	3.088E+08
R01863	reaction	inosine:phosphate alpha-D-ribosyltransferase	7.366E-03
R01867	reaction	(S)-dihydroorotate:fumarate oxidoreductase	1.035E-03
R01876	reaction	uridine:phosphate alpha-D-ribosyltransferase	2.008E-03
R01969	reaction	Deoxyguanosine:orthophosphate ribosyltransfer...	1.000E-06
R02147	reaction	guanosine:phosphate alpha-D-ribosyltransferas...	1.837E-02
R02164	reaction	succinate:quinone oxidoreductase	1.000E-06
R02294	reaction	N-Ribosylnicotinamide:orthophosphate ribosylt...	4.332E-02
R02296	reaction	cytidine:orthophosphate alpha-D-ribosyltransf...	3.703E-02
R02297	reaction	Xanthosine:orthophosphate ribosyltransferase	4.035E-02
R02313	reaction	N6-(L-1,3-Dicarboxypropyl)-L-lysine:NAD+ oxid...	1.000E-06
R02315	reaction	N6-(L-1,3-Dicarboxypropyl)-L-lysine:NADP+ oxi...	1.000E-06
R02317	reaction	(S)-2-amino-6-oxohexanoate hydro-lyase (spont...	1.000E-06
R02340	reaction	(1S,2R)-1-C-(indol-3-yl)glycerol 3-phosphate ...	7.357E-03
R02409	reaction	Coenzyme A:oxidized-glutathione oxidoreductas...	4.474E-02
R02484	reaction	deoxyuridine:orthophosphate 2-deoxy-D-ribosyl...	1.000E-06
R02557	reaction	Deoxyadenosine:orthophosphate ribosyltransfer...	1.000E-06
R02722	reaction	L-serine hydro-lyase [adding 1-C-(indol-3-yl)...	3.011E-03
R02748	reaction	Deoxyinosine:orthophosphate ribosyltransferas...	1.000E-06
R02749	reaction	2-deoxy-D-ribose 1-phosphate 1,5-phosphomutas...	1.000E-06

R03102	reaction	L-2-aminoadipate-6-semialdehyde:NAD+ 6-oxidor...	1.000E-06
R03103	reaction	L-2-aminoadipate-6-semialdehyde:NADP+ 6-oxido...	1.000E-06
R03217	reaction	O-Acetyl-L-homoserine succinate-lyase (adding...	3.059E-02
R03260	reaction	O-Succinyl-L-homoserine succinate-lyase (addi...	2.438E-03
R03524	reaction	L-cysteine hydrogen-sulfide-lyase (adding HCN...	3.504E-02
R03896	reaction	(R)-2-Methylmalate hydro-lyase (2-methylmalea...	1.149E+08
R03898	reaction	2-methylmaleate hydratase	1.000E-06
R03968	reaction	2-Isopropylmalate hydro-lyase	1.000E-06
R04001	reaction	3-Isopropylmalate hydro-lyase	1.000E-06
R04390	reaction	L-2-aminoadipate-6-semialdehyde:NADP+ 6-oxido...	2.104E-02
R04426	reaction	(2R,3S)-3-isopropylmalate:NAD+ oxidoreductase	1.000E-06
R04559	reaction	1-(5'-Phosphoribosyl)-5-amino-4-(N-succinocar...	7.225E-03
R05598	reaction	Benzylsuccinate fumarate-lyase	1.083E-02
R05605	reaction	2-dehydro-3-deoxy-6-phospho-D-gluconate D-gly...	2.199E-03
R05636	reaction	1-Deoxy-D-xylulose-5-phosphate pyruvate-lyase...	3.417E-03
R06531	reaction	ATP:L-threonine O-phosphotransferase	2.361E-04
R06590	reaction	sedoheptulose-7-phosphate:D-glyceraldehyde-3-...	1.654E-02
R06789	reaction	(2Z,4E,7E)-2-Hydroxy-6-oxonona-2,4,7-triene-1...	1.163E-02
R06903	reaction	2-Methylnaphthalene + Fumarate <=> 2-Naphtylm...	2.194E-02
R06987	reaction	propanoyl-CoA:formate C-propanoyltransferase	2.218E-02
R07159	reaction	D-glyceraldehyde-3-phosphate:ferredoxin oxido...	1.000E-06

R07274	reaction	O-phospho-L-serine:hydrogen-sulfide 2-amino-2...	1.948E-04
R07399	reaction	Acetyl-CoA + Pyruvate + H2O <=> (R)-2-Methylm...	2.986E-03
R07456	reaction	D-ribulose 5-phosphate,D-glyceraldehyde 3-pho...	3.194E+09
R08323	reaction	7-Mercaptoheptanoic acid + L-Threonine + ATP ...	5.991E-03
R08555	reaction	(R)-lactate hydro-lyase (adding N-acetyl-D-gl...	9.758E-03
R08559	reaction	protein-N(pi)-phosphohistidine:N-acetylmurama...	1.000E-06
R10049	reaction	2-oxopropanal:D-fructose 1,6-bisphosphate gly...	4.546E-02
R10052	reaction	(2R,3S)-3-isopropylmalate:NAD+ oxidoreductase	1.000E-06
R10090	reaction	citrate:N6-acetyl-N6-hydroxy-L-lysine ligase ...	6.270E-03
R10170	reaction	(2R,3S)-3-isopropylmalate hydro-lyase (2-isop...	1.000E-06
R10270	reaction	(5R)-5-phosphooxy-L-lysine phosphate-lyase (d...	4.432E-04
R10343	reaction	succinyl-CoA:acetate CoA-transferase	1.608E-03
R10660	reaction	fumarate CoM:CoB oxidoreductase (succinate fo...	6.353E+09
R10677	reaction	citrate:L-glutamate ligase (ADP-forming)	2.358E-02
R10699	reaction	L-lysine:8-amino-7-oxononanoate aminotransfer...	1.201E-03
R10860	reaction	D-glyceraldehyde-3-phosphate:NAD+ oxidoreduct...	1.000E-06
R10888	reaction	C20914 + L-Threonine <=> C20915	1.339E-02
R10891	reaction	Tabtoxin + H2O <=> Tabtoxinine-beta-lactam + ...	1.168E-03
R10892	reaction	tabtoxinine-beta-lactam:L-threonine ligase (A...	8.832E-04
R10940	reaction	fumarate:L-2,3-diaminopropanoate ligase (AMP-...	6.289E-03
R10973	reaction	D-ribose-2,5-bisphosphate 2-phosphohydrolase	2.912E-03
R11024	reaction	ATP:N-acetyl-D-muramate 1-phosphotransferase	1.000E-06
R11679	reaction	(S)-2-amino-6-oxohexanoate:NADP+ oxidoreducta...	1.000E-06

R11785	reaction	N-acetyl-D-muramate 6-phosphate phosphohydrol...	1.000E-06
R12308	reaction	L-2,3-diaminopropanoate:citrate ligase (2-[(L...	2.769E-03
R12353	reaction	D-Ornithine + Citrate + ATP <=> N5-Citryl-D-o...	4.337E-04
R12354	reaction	N5-Citryl-D-ornithine + Citrate + ATP <=> Sta...	3.695E-02
R12596	reaction	Spermidine + Citrate + ATP <=> N-Citryl-sperm...	2.685E-04
C00009	compound	Orthophosphate	9.902E-03
C00042	compound	Succinate	1.000E-06
C00058	compound	Formate	1.695E-02
C00073	compound	L-Methionine	3.505E-03
C00097	compound	L-Cysteine	1.000E-06
C00109	compound	2-Oxobutanoate	1.133E-02
C00117	compound	D-Ribose 5-phosphate	1.000E-06
C00118	compound	D-Glyceraldehyde 3-phosphate	1.000E-06
C00122	compound	Fumarate	1.000E-06
C00141	compound	3-Methyl-2-oxobutanoic acid	2.304E-02
C00158	compound	Citrate	1.000E-06
C00188	compound	L-Threonine	1.000E-06
C00672	compound	2-Deoxy-D-ribose 1-phosphate	1.000E-06
C00673	compound	2-Deoxy-D-ribose 5-phosphate	2.442E-02
C02226	compound	2-Methylmaleate	3.627E-04
C02504	compound	alpha-Isopropylmalate	1.000E-06
C02631	compound	2-Isopropylmaleate	1.000E-06
C02713	compound	N-Acetylmuramate	1.000E-06
C03145	compound	N-Formylmethionine	1.000E-06

C04076	compound	L-2-Aminoadipate 6-semialdehyde	1.000E-06
C04411	compound	(2R,3S)-3-Isopropylmalate	1.000E-06
C06032	compound	D-erythro-3-Methylmalate	1.000E-06
C16698	compound	N-Acetylmuramic acid 6-phosphate	2.110E-03

1017